Pflugers Arch - Eur J Physiol (2017) 469:1631–1649
DOI 10.1007/s00424-017-2037-4

NEUROSCIENCE

Effect of temperature on FAD and NADH-derived signals and neurometabolic coupling in the mouse auditory and motor cortex

Baher A. Ibrahim[1,2] · **Huan Wang**[3,4,5,6] · **Alexandria M. H. Lesicko**[7] · **Bethany Bucci**[1,2] · **Kush Paul**[2] · **Daniel A. Llano**[1,2,3,4,7]

Received: 4 May 2017 / Revised: 3 July 2017 / Accepted: 13 July 2017 / Published online: 7 August 2017

Abstract Tight coupling of neuronal metabolism to synaptic activity is critical to ensure that the supply of metabolic substrates meets the demands of neuronal signaling. Given the impact of temperature on metabolism, and the wide fluctuations of brain temperature observed during clinical hypothermia, we examined the effect of temperature on neurometabolic coupling. Intrinsic fluorescence signals of the oxidized form of flavin adenine dinucleotide (FAD) and the reduced form of nicotinamide adenine dinucleotide (NADH), and their ratios, were measured to assess neural metabolic state and local field potentials were recorded to measure synaptic activity in the mouse brain. Brain slice preparations were used to remove the potential impacts of blood flow. Tight coupling between metabolic signals and local field potential amplitudes was observed at a range of temperatures below 29 °C. However, above 29 °C, the metabolic and synaptic signatures diverged such that FAD signals were diminished, but local field potentials retained their amplitude. It was also observed that the declines in the FAD signals seen at high temperatures (and hence the decoupling between synaptic and metabolic events) are driven by low FAD availability at high temperatures. These data suggest that neurometabolic coupling, thought to be critical for ensuring the metabolic health of the brain, may show temperature dependence, and is related to temperature-dependent changes in FAD supplies.

Keywords Neurometabolic coupling · Flavoprotein imaging · Temperature · Hypothermia · Auditory cortex · Hippocampus

✉ Daniel A. Llano
d-llano@illinois.edu

[1] Department of Molecular and Integrative Physiology, University of Illinois at Urbana-Champaign, Urbana, IL, USA

[2] The Beckman Institute for Advanced Science and Technology, University of Illinois at Urbana-Champaign, 405 North Mathews Avenue, Urbana, IL 61801, USA

[3] College of Medicine, University of Illinois at Urbana-Champaign, Urbana, IL, USA

[4] Carle Neuroscience Institute, Carle Foundation Hospital, Urbana, IL, USA

[5] Re3 Innovative Neuroscience Institute, P.L.L.C, Sarasota, FL, USA

[6] Re3 Stem Cell and Healing Institute, P.L.L.C, Sarasota, FL, USA

[7] Neuroscience Program, University of Illinois at Urbana-Champaign, Urbana, IL, USA

Introduction

One century ago, Roy and Sherrington showed the coupling between neuronal activity and the delivery of energy through the cerebral vasculature [84]. In addition, metabolic dysfunction was shown to impair synaptic transmission or cell viability in many brain preparations [12, 50, 51, 60, 87, 105]. Currently, most brain functional imaging techniques are conducted based on neurometabolic coupling theory [62]. Yet, the mechanisms linking brain activity to metabolism, and the impact of important physiological parameters, such as temperature, on neurometabolic coupling remain poorly understood. Given the high rate of metabolism and consequent heat production that occurs in the brain, fluctuations in local brain temperature can span up to 2–3 °C degrees (reviewed in Wang et al. [104]). Furthermore, therapeutically, hypothermia has received increasingly intense clinical attention to protect against some brain injuries [5, 25, 37, 73, 90]. Therefore, it is critical to understand how

brain temperature affects synaptic and metabolic activity in the brain. Previous studies have shown that neuronal resting membrane potential, the rate of neuronal firing, and the onset of depolarization and repolarization are temperature-dependent processes [55, 103]. However, these studies did not simultaneously measure the impact of temperature on cellular metabolism which could have modulated neuronal activity [38]. In contrast, many in vivo and ex vivo studies examined the impact of the temperature on cerebral blood flow and metabolic rate during hypoxia versus normal conditions [19, 71, 75, 106], but they did not simultaneously measure the impact of temperature on the neuronal activity. Given the previous work demonstrating that temperature could impact both brain metabolism and neural activity, and the different metabolic demands that exist at different temperatures [8, 19, 49, 78, 103], we hypothesized that the coupling between neural activity and metabolic activity may be temperature-dependent. To test this hypothesis, we simultaneously recorded local field potentials and endogenous metabolic signals such as oxidized flavin adenine dinucleotide (FAD^{++}) and reduced nicotinamide adenine dinucleotide (NADH) across different temperatures. The oxidized (FAD^{++}/NAD^{+}) or the reduced ($FADH_2$/NADH) forms of these coenzymes are directly involved in ATP production [67]. Delivering the electrons by these coenzymes is associated with the oxidation of both $FADH_2$ and NADH to FAD^{++} (henceforth, FAD) and NAD^{+} (henceforth, NAD), respectively, which leads to the increase of FAD and the decrease of NADH signals upon each neuronal activation [39]. In addition to their use in the diagnoses of some diseases like myocardial infarction and cancer [56, 79], the fluorescence associated with FAD and NADH was previously characterized to measure metabolic activity in the brain tissue [42, 57, 66, 80, 91, 101]. Stimulation of mitochondrial oxidative phosphorylation is induced by the influx of calcium ions upon synaptic transmission, and approximately 80% of FAD signals come from postsynaptic activation [57, 80, 91]. As such, flavoprotein fluorescence imaging has been reported as a highly quantitative marker for neuronal and synaptic activity with a high degree of stability over hours [57, 58, 81, 91, 92, 100]. Given that FAD and NADH represent different oxidative states, have signals that contain temporally different components [light vs dark phase (peak vs undershoot) of FAD signals] [82], and own different excitation and emission spectra [67], tracking the change of FAD and NADH signals was considered an effective tool to test our hypothesis. Brain slices are a particularly useful tool for these studies since the impact of blood flow, which may dissipate heat and alter the metabolic milieu, is removed, providing the experimenter with complete control of the temperature and metabolic environment of the brain tissue.

Material and methods

Subjects

Adult (2–4 months) BALB/c mice (Jackson Laboratory) of both sexes were used. All applicable international, national, and/or institutional guidelines for the care and use of animals were followed. All surgical procedures were approved by the Institutional Animal Care and Use Committee (IACUC) at University of Illinois Urbana-Champaign. Animals were housed in animal care facilities approved by the American Association for Accreditation of Laboratory Animal Care (AAALAC). ARRIVE guidelines (Reporting in Vivo Experiments) were followed. Since each animal served as its own control, there was no randomization or blinding done.

Brain slicing

Mice were initially anesthetized with ketamine (100 mg/kg) and xylazine (3 mg/kg) intraperitoneally and transcardially perfused with chilled (4 °C) sucrose-based slicing solution containing the following (in mM): 234 sucrose, 11 glucose, 26 $NaHCO_3$, 2.5 KCl, 1.25 NaH_2PO_4, 10 $MgCl_2$, 0.5 $CaCl_2$. From the first group of mice, 600 μm thick auditory thalamocortical brain slices were obtained [14, 96]. For the second group of mice, guided by Allen brain atlas (http://www.brain-map.org/), 500 μm coronal slices were obtained at (+1.145 to −0.18 mm) from bregma to examine FAD and local field potential (LFP) signals of the spontaneous activity of layer 2/3 of the motor cortex. To elicit the spontaneous activity of the neuronal network, SR-95531 (Tocris, 1262, gabazine) was used to block the inhibitory inputs through its $GABA_A$ receptor blocking effect as shown before [107]. To examine the resting redox ratio under (cooling vs rewarming) or (normal vs hypoxic) conditions of the cortex, hippocampus, and thalamus, 500 μm coronal slices were obtained from a third group of mice at (−2.88 to −3.45 mm) from bregma. All slices were incubated for 30 min in 33 °C incubation solution (in mM: 26 $NaHCO_3$, 2.5 KCl, 10 glucose, 126 NaCl, 1.25 NaH_2PO_4, 3 $MgCl_2$, and 1 $CaCl_2$). After incubation, slices were transferred to a perfusion chamber coupled to an upright Olympus BX50 microscope, perfused with artificial cerebrospinal fluid (ACSF) containing (in mM) 26 $NaHCO_3$, 2.5 KCl, 10 glucose, 126 NaCl, 1.25 NaH_2PO_4, 2 $MgCl_2$, and 2 $CaCl_2$, and bubbled with 95% oxygen/5% carbon dioxide. To avoid the negative impact of liquid flow turbulence on optical imaging, the flow rate was set to be between 3 and 6 ml per min. The slice was elevated from the bottom of the chamber by placing it on a mesh to deliver adequate oxygenation and drug perfusion to both surfaces of the slice [29, 30].

Temperature modulation

The temperature in the imaging chamber was adjusted by a dual in-line heater/cooler probe SC-20 which was controlled by bipolar temperature controller CL-100 (Warner Instruments, Connecticut, USA). The temperature of the brain slice was changed either from 37 to 9 °C or from 9 to 37 °C in 4 °C intervals. The temperature was automatically adjusted by a feedback thermometer which was located in the bath adjacent to the brain slice. Before taking any measurements, brain slices were kept 5 min at each temperature.

Changes in oxygen tension

Oxygen concentration was manipulated with a mixture of oxygen and nitrogen gases while keeping CO_2 at a constant level at (5%) to maintain a stable pH. A dissolved oxygen meter, inO_2 (Innovative Instruments, Inc), was used to measure oxygen concentration in ACSF. The oxygen meter was calibrated at 21 and at 37 °C individually, using ACSF perfused with 95% nitrogen/5% CO_2 gas mixture for the minimum calibration point and with 95% oxygen/5% CO_2 for the maximum calibration point. The bubbling rate of O_2 and N_2 gases was altered to adjust the oxygen concentration of the ACSF.

Slice stimulation

One second long trains of electrical pulses (300 μA, 40 Hz, 1 ms pulse width) were sent to the subcortical white matter of thalamocortical slices by a tungsten monopolar electrode every 20 s. The electrical parameters meet the lowest duty cycle that is required for the clearance of free radicals produced by electrical stimulation as reported in Varela et al. review [99]. In addition, this electrical paradigm generates consistent FAD signals as shown previously [59, 95, 96]. The parameters of the electrical pulses were adjusted by a B&K precision wave generator (model # 4063) and World Precision Instruments stimulation isolator (A-360). The stimulation was repeated five times with a 20-s delay before the first stimulation. To test the physiological reliability of FAD imaging as a quantitative tool for the neuronal activity, LFP signals were recorded from the auditory cortex after sending one electrical pulse (1 ms long) at different current amplitudes (100–500 μA) to the white matter.

Electrophysiology

The change of FAD signals of auditory cortex (evoked by electrical stimulation of the white matter) or motor cortex (evoked by SR-95531) was simultaneously imaged with extracellular and/or intracellular recordings. For extracellular recording, a low-impedance (~10 μm diameter) glass electrode filled with ACSF was placed into layer 4 of auditory cortex or layer 2/3 of the motor cortex to measure LFP signals. LFP signals from auditory or motor cortex were amplified 10,000 or 1000 times under 300 or 100 Hz high cutoff frequency, respectively, using a Dagan 2400 extracellular preamplifier and recorded using a PowerLab digitizer (AD Instruments). LabChart software (v.8) was used to capture the digitized LFP signals from auditory or motor cortex with 20 or 10 kHz sampling rate, respectively. The raw LFP signals were digitally filtered at a bandwidth of 1 to 100 Hz offline. A 30-ms smoothing window was applied to LFP signals from auditory cortex offline. Whole-cell recording was performed using a visualized slice setup outfitted with infrared-differential interference contrast optics. Recording pipettes were pulled from borosilicate glass capillary tubes and had tip resistances of 2–5 MΩ when filled with intracellular solution, which contained the following (in mM: 117 K-gluconate, 13 KCl, 1.0 $MgCl_2$, 0.07 $CaCl_2$, 0.1 ethyleneglycol-bis(2-aminoethylether)-N,N,N′,N′-tetra acetic acid, 10.0 4-(2-hydroxyethyl)-1-piperazineethanesulfonic acid, 2.0 Na-ATP, 0.4 Na-GTP, and 0.5% biocytin, pH 7.3). A Multiclamp 700B amplifier and pClamp software (Molecular Devices) were used for data acquisition (20 kHz sampling).

Imaging and analysis

From the brain slice, the oxidized FAD and the reduced NADH endogenous fluorescence signals were measured. FAD signals were measured using a stable DC fluorescence illuminator (Prior Lumen 200) and a U-M49002Xl E-GFP Olympus filter cube set [excitation: 470–490 nm, dichroic 505 nm, emission 515 nm long pass]. NADH imaging was performed using a custom filter cube [excitation: 357/44 nm (BrightLine® bandpass filter, FF01-357/44-25, Semrock), dichroic 400 long pass (xf2001-400DCLP, Omega Optical), emission 440/40 nm (BrightLine® bandpass filter, FF01-440/40-25-STR, Semrock)]. All data were collected using an infinity-corrected Olympus MacroXL ×4 objective (NA 0.28) and OptiMOS camera (QImaging) using 4 × 4 binning (with resulting image size of 348 × 270 pixels) and Micro-Manager software [18]. For all imaging experiments, movies were simultaneously obtained with electric stimulation or LFP recording at 4 frames per second. A region of interest (ROI) was created, and the responses associated with evoked activity were expressed as a change in fluorescence over baseline fluorescence ($\Delta f/f$). In the cases of the electrically evoked synaptic activity, an ROI was placed in the auditory cortex. $\Delta f/f$ of both FAD and NADH signals associated with evoked activity was calculated with custom-written MATLAB software. For FAD signals associated with spontaneous depolarization (SPD) events, the ROI was placed directly superficial to the site of LFP recording. Because of the random nature of the occurrence and the amplitude of SPD events, LFP and $\Delta f/f$ measurements associated with each event were calculated manually using LabChart 8 and

OriginPro software, respectively. For the assessment of the redox ratios, both FAD and NADH signals were imaged using the same imaging parameters. To examine the effect of temperature on the fluorescence of FAD and NADH compounds themselves, the fluorescence of 9.2 μM of FAD (Sigma, F6625-25MG) and NADH (Roche Diagnostics, 10128023001) compounds dissolved in ACSF was measured across different temperatures using the same imaging setup and temperature modulation used in the slice experiments. These data were used to normalize the endogenous FAD and NADH fluorescence signals as well as the redox ratios.

Induction of hypoxia

Hypoxic conditions were induced by using ACSF perfused with (95% nitrogen/5% CO_2). Hypoxia was used to inhibit oxidation reactions and obtain the ceiling of NADH signals and the floor of FAD signals [23]. Both FAD and NADH signals of the brain slices at normal versus hypoxic condition were imaged, and the redox ratio was then calculated for each condition at different temperatures. % of oxidative capacity was calculated using:

$$\%\ of\ oxidative\ capacity = \left[\left(\frac{(redox\ ratio\ under\ normoxic\ conditions - redox\ ratio\ under\ hypoxic\ conditions)}{redox\ ratio\ under\ hypoxic\ conditions}\right) \times 100\%\right]$$

Statistics

One-way repeated measure ANOVA was used to evaluate $\Delta f/f$ values associated with electrically evoked activity and redox ratio under each individual condition. To do this, the average of $\Delta f/f$ values of FAD or NADH signals resulting from five stimuli at each temperature was compared at different temperatures. Due to the spontaneous nature of SPD events, we compared them as individual events using one-way ANOVA to evaluate their frequency and LFP amplitude as well as FAD signal components including $\Delta f/f$, FAD signal peak amplitude, FAD signal undershoot amplitude, and peak to peak (the difference between FAD signal peak and undershoot) at different temperatures. Paired *t* test was used only to compare different oxygen saturated ACSF solutions. Two-way repeated measures ANOVA was used only to compare between different brain structures or between different oxidative capacities across different temperatures. Fisher least significant difference (LSD) post-test was used for pairwise comparison. Effects were considered significant when $p \leq 0.05$. The statistical analysis and plotting of graphs were done by OriginPro 2016 software. Based on the confidence limits calculated by (mean ± 2SDs), the identified outliers, which were higher than ±2SDs in both directions, were excluded from the statistical analysis as follows; (LFP, $N = 9$, SDs used = 5, eliminated outliers = 14 out of $n = 352$), ($\Delta f/f$, $N = 9$, SDs used = 4, eliminated outliers = 12 out of $n = 322$), (FAD signal peak amplitude, $N = 6$, SDs used = 3, eliminated outliers = 6 out of $n = 199$), (FAD signal undershoot amplitude, $N = 6$, SDs used = 2, eliminated outliers = 2 out of $n = 67$), and (peak to peak, $N = 6$, SDs used = 2, eliminated outliers = 2 out of $n = 67$). Throughout the manuscript, N = number of slices used while n = number of events analyzed. In all cases, a single slice was used from each mouse.

Artworks

All artwork graphics were made using Origin Pro for line art and Adobe illustrator for arranging the combination art images.

Results

The metabolic signals associated with synaptic activity are temperature-dependent

Endogenous FAD and NADH signals were used to track neuronal activity in the auditory cortex after electrically stimulating the subcortical white matter in auditory thalamocortical slices [14, 59, 96]. Here, sending electric stimulation to the white matter evoked synaptic activity in the auditory cortex which was associated with an increase of the FAD signal (Fig. 1a). The change of FAD signals induced by the electrical stimulation was temporally matched with LFP signals (Fig. 1b). Both plots of calculated $\Delta f/f$ of FAD and the amplitude of LFP signals derived from auditory cortex after the electrical stimulation of white matter adopted a linear relationship with current amplitude (Fig. 1c). The significant correlation between $\Delta f/f$ of FAD and the amplitude of LFP signals (Fig. 1d) implicated the physiological sensitivity of FAD signals to track the neuronal activity. At high temperatures (≥29 °C) the electrical stimulation of the white matter drove a biphasic change of both FAD and NADH signals of the auditory cortex. Each electrical stimulation was followed by FAD signal peak (oxidation of $FADH_2$ to FAD) then FAD signal undershoot (reduction of FAD to $FADH_2$) or NADH signal dip (oxidation of NADH to NAD) then NADH signal overshoot (reduction of NAD to NADH). In contrast, a monophasic change of both

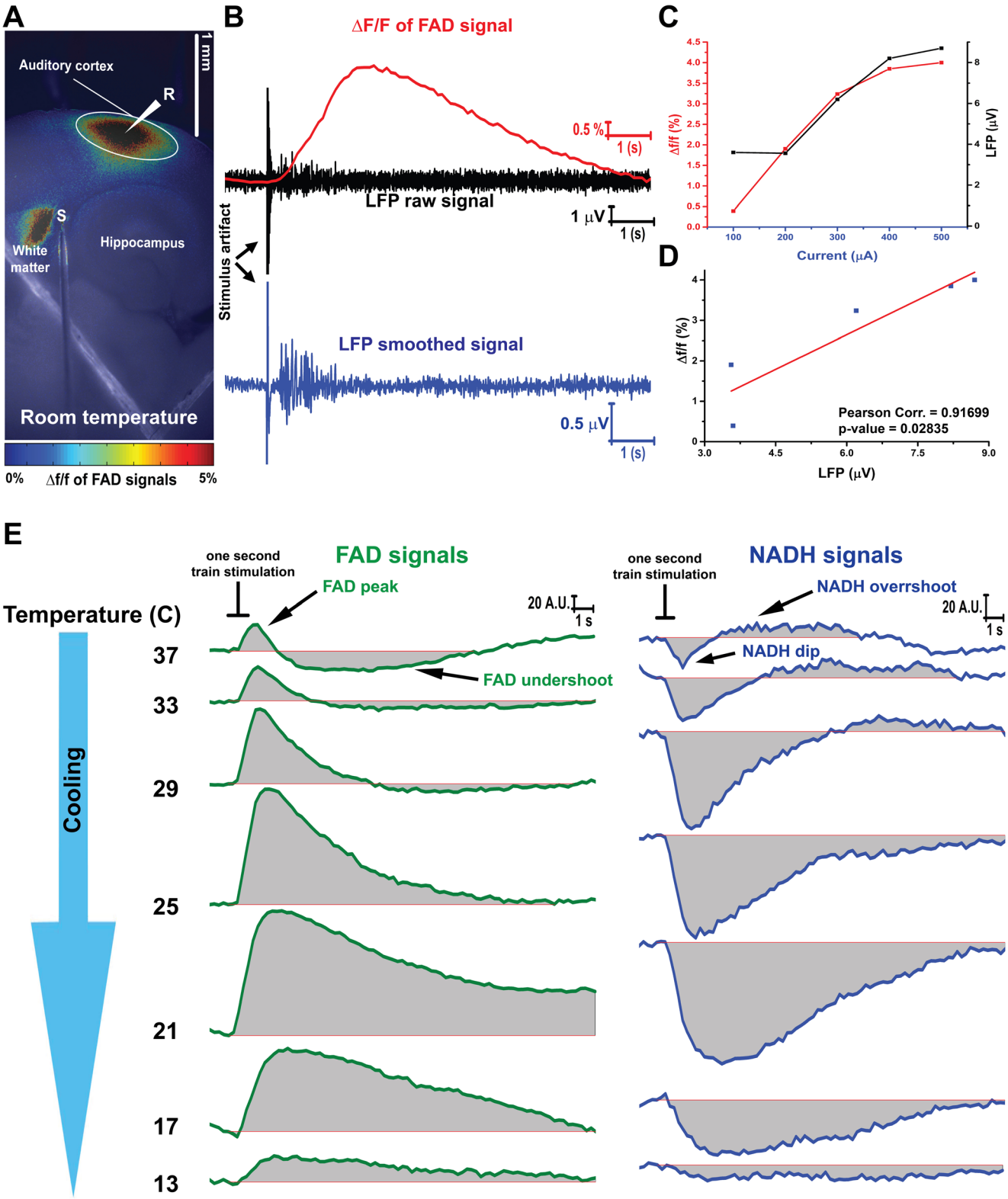

Fig. 1 FAD and NADH signals associated with the electric stimulation of white matter at 25 °C: **a** pseudocolor heat map of the average intensity of the Δ*f*/*f* of FAD signals evoked by the electrical stimulation of subcortical white matter of auditory thalamocortical brain slice at room temperature; *S*, the stimulation site; *R*, LFP recording site; *white circle*, the region of interest (ROI) used to quantify Δ*f*/*f* of FAD signals; **b** time traces of FAD (*top panel*, *red*), LFP raw (*top panel*, *black*), and LFP smoothed (*bottom panel*, *blue*) signals of the auditory cortex after electrical stimulation of subcortical white matter at room temperature; **c** merged plots of LFP and Δ*f*/*f* of FAD signals with increasing current; **d** Pearson correlation plot between LFP and Δ*f*/*f* of FAD signals; **e** the change of raw FAD (*right panel*, *green lines*) and NADH (*left panel*, *blue lines*) signals of the auditory cortex at different temperatures after electrical stimulation of subcortical white matter; *black lines*, the duration of the electrical train (1 s)

FAD (FAD signal peak) and NADH (NADH signal dip) were only shown at lower temperatures (≤25 °C) after electrical stimulation (Fig. 1e).

$\Delta f/f$ for both FAD and NADH responses was then calculated across temperatures (Fig. 2). Regardless the direction of temperature change (cooling vs warming), FAD signal amplitude was strongly temperature-dependent with a maximum value at 25 °C and minimum values at lower or higher temperature (Fig. 2a). Cooling from 37 °C increased the $\Delta f/f$ of FAD, until a maximum value at 25 °C (Fig. 2b, $N = 4$, $f(6,18) = 27.3$, $p = 4.16 \times 10^{-8}$), then decreased with cooling below 21 °C. Similarly, cooling increased $\Delta f/f$ of NADH signals, but in the negative direction, until it reached its maximum absolute value at 29 °C (Fig. 2c, $N = 3$, $f(6,12) = 11.68$, $p = 2.09 \times 10^{-4}$), then decreased with further cooling below 21 °C. Warming the slice from 13 °C increased both $\Delta f/f$ of FAD and NADH signals (Fig. 2e, f, $N = 4$ and 3; $f(6,18) = 16.96$ and $f(6,12) = 19.48$; $p = 1.6 \times 10^{-6}$ and $p = 1.54 \times 10^{-5}$ for FAD and NADH signals, respectively) until they reached their maximum level at 25 °C, then diminished by further warming above 25 °C. Merging the $\Delta f/f$ values of FAD and NADH signals at both conditions (cooling and warming) showed that the maximum of $\Delta f/f$ values of both signals evoked by synaptic activity were observed at 25 °C (red line, Fig. 2d, g) such that $\Delta f/f$ of FAD signals evoked by the synaptic activity at 37 °C significantly dropped by 85% from that at room temperature (21 °C) (Fig. 2h, i, $N = 4$, $t = 5.1$, $p = 0.007$).

To determine if the drop in the change in the FAD signal was due to the lower solubility of oxygen at 37 °C compared to room temperature, the oxygen concentration at room temperature was adjusted to approximate the oxygen concentration at 37 °C. This adjustment lowered ACSF oxygen saturation by 27%. Our results showed a non-significant decline $\Delta f/f$ of FAD signals derived by electrically evoked synaptic activity in the auditory cortex at both oxygen levels at room temperature (Fig. 2j). In contrast with the temperature data, ACSF with diminished oxygen at room temperature reduced $\Delta f/f$ of FAD signals by 22.1% compared to that obtained under ACSF saturated with 100% oxygen (Fig. 2k, $p = 0.11$). These data suggest that the effect of temperature on metabolism is not due to a drop in the oxygen concentration at 37 °C.

Neurometabolic coupling is temperature-dependent

In the presence of 4 μM SR95531, spontaneous activations were observed with FAD imaging, consisting of a relatively sharp rise in fluorescence, peaking at about 1 s after baseline, with a slow decline, returning to baseline after about 5–10 s (Fig. 3b, c, red trace). To determine the nature of these events, LFPs were also measured during spontaneous events and revealed a brief (50 ms) negative peak seen consistently in association with optical events (Fig. 3c, black trace). Simultaneous recording of whole-cell voltage revealed a sharp depolarization crowned with an action potential followed by a sustained depolarization (Fig. 3c, blue trace). These electrical events strongly resemble the extra- and intracellular manifestations of paroxysmal depolarizing events, respectively [43, 97, 98, 107], and therefore, we refer to them as SPDs.

LFP and FAD signals of the SPD events in layer 2/3 of the cortex demonstrated a highly synchronized pattern between their time traces across different temperatures (Fig. 4a). As before, superimposed pseudocolored images were made to demonstrate the fluorescence intensity of FAD signals associated with SPD events. The merged image also showed the site of LFP recording electrode (Fig. 4b). The expansion of an individual FAD signal shows the known prominent two phases of FAD signal (above vs below baseline) which were assigned as light (FAD signal peak) versus dark (FAD signal undershoot) phases, respectively (Fig. 4c), as seen previously in other brain preparations [13, 22, 81]. The impacts of temperature on the components of FAD signal, the amplitude and frequency of the SPDs, and the coupling between electrical and metabolic signals were also investigated (Fig. 5). We observed no SPD events in the presence of SR-95531 at 37 °C, as indicated by both LFP or FAD time traces (Fig. 4a).

Cooling increased the number of SPD events until their maximum number at 17 °C, beyond which they significantly decreased in frequency upon further cooling to 13 °C (Fig. 5a, $N = 9$; $F(6, 62) = 52.5$; $p < 1 \times 10^{-9}$). Because of the absence of detected events at 37 °C, data from this temperature point were excluded from the subsequent analysis. Similar to previous data [1], the maximum LFP amplitude was observed at 33 °C, and remained constant with cooling until 25 °C, below which it decreased significantly with subsequent cooling to 13 °C (Fig. 5b, $N = 9$, $n = 352$; $F(5, 351) = 208.1$; $p < 1 \times 10^{-9}$). Consistent with the profile of $\Delta f/f$ of FAD signals evoked after electric stimulation under cooling (Fig. 2b), the amplitude of $\Delta f/f$ of FAD signals followed the same profile. Cooling the brain slice below 37 °C increased the amplitude of $\Delta f/f$ of FAD significantly until it reached its maximum level at 25 °C. Further cooling below 25 °C reduced $\Delta f/f$ of FAD signals significantly until it reached its minimum level at 13 °C (Fig. 5c, $N = 9$, $n = 322$; $F(5, 321) = 153.6$; $p < 1 \times 10^{-9}$). Separation between the $\Delta f/f$ of FAD and the LFP amplitudes was observed at temperatures above 29 °C, implicating the presence of neurometabolic decoupling at those temperatures (Fig. 5d, gray box). In contrast, a strong degree of neurometabolic coupling was observed at lower temperatures which was indicated by a complete overlap between $\Delta f/f$ of FAD signals and LFP amplitudes at 25 °C or below (Fig. 5d). Both the FAD signal peak and the undershoot had their maximum excursions at intermediate temperatures, but

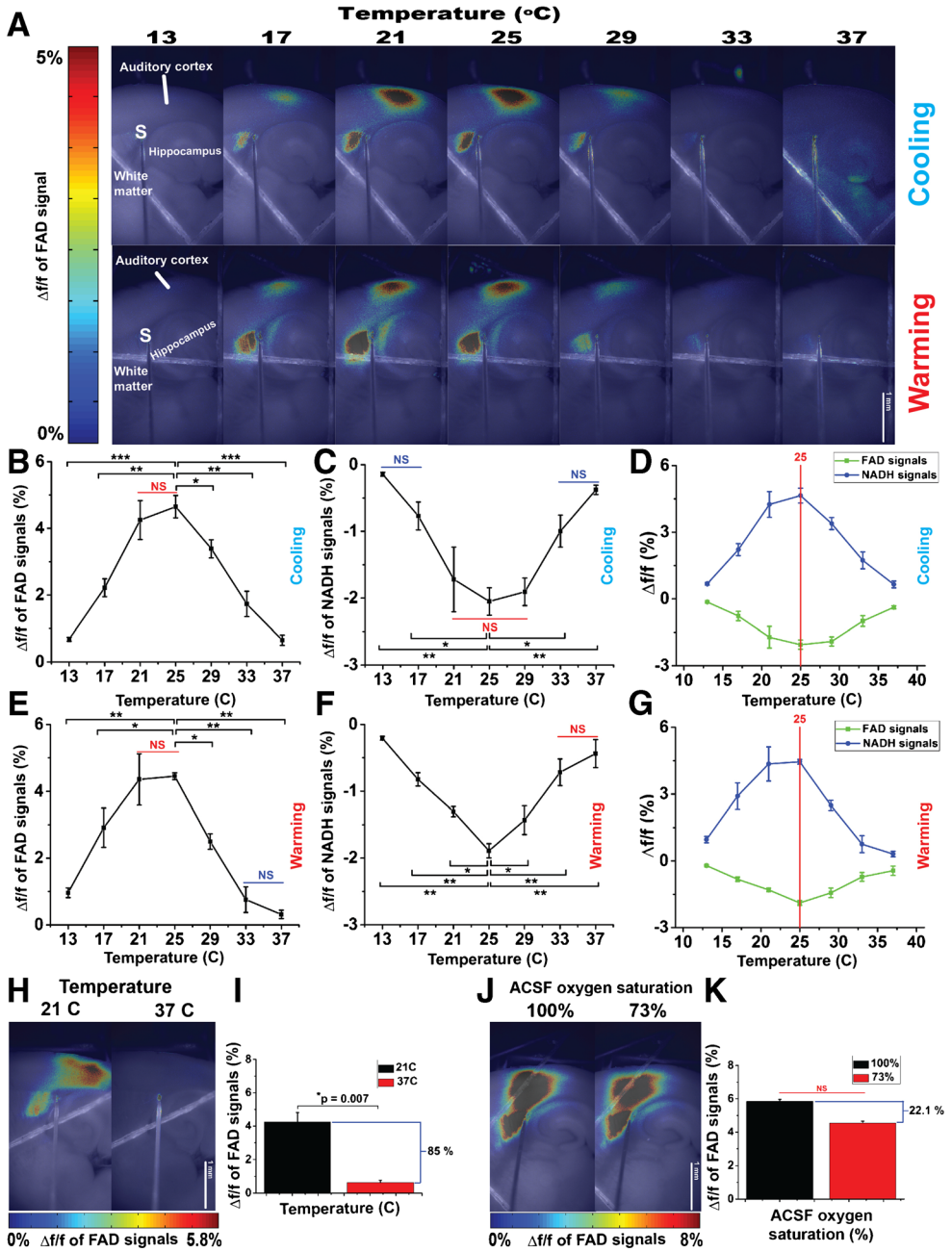

Fig. 2 The metabolic signals associated with synaptic activity are temperature-dependent: **a** pseudocolor heat map of the average intensity of the $\Delta f/f$ of FAD signals evoked by the electrical stimulation of subcortical white matter of auditory thalamocortical brain slice at different temperatures under cooling (*top panel*) and warming (*bottom panel*); *S*, site of stimulating electrode; **b**, **e** line plots between temperature (*x*-axis) and $\Delta f/f$ of FAD signals associated with synaptic activity (*y*-axis) under cooling and warming, respectively; **c**, **f** line plots between temperature (*x*-axis) and $\Delta f/f$ of NADH signals associated with synaptic activity (*y*-axis) under cooling and warming, respectively; **d**, **g** merged plots of $\Delta f/f$ of both FAD and NADH under cooling and warming, respectively, *red line* shows the maximum values of $\Delta f/f$ of both signals; **h**, **j** pseudocolor heat map of the average intensity of the $\Delta f/f$ of FAD signals associated with synaptic activity at (21 vs. 37 °C) and at (100 vs. 73%) oxygen saturated ACSF, respectively; **i** bar plots of $\Delta f/f$ of FAD signals associated with synaptic activity at 21 °C (*black bar*) vs 37 °C (*red bar*); **k** bar plots of $\Delta f/f$ of FAD signals associated with synaptic activity under 100% (*black bar*) vs 73% (*red bar*) oxygen saturated ACSF at 21 °C; $N = 4$ (one slice per mouse); post hoc, *vs 25 °C ($0.05 > p > 1 \times 10^{-4}$), **vs 25 °C ($1 \times 10^{-4} > p > 1 \times 10^{-7}$), ***vs 25 °C ($1 \times 10^{-7} > p > 1 \times 10^{-9}$); *NS*, non-significant difference between temperatures covered with a *solid line*

in opposite directions and with maximum values at different temperatures.

At high temperatures, the dominant FAD excursion during SPDs was in the negative direction, similar to previous data from the hippocampus (Fig. 4a) [40]. Cooling increased both FAD signal peak and undershoot amplitudes until they reached their maximum absolute values at 25 °C for FAD signal peak and 29 °C for FAD signal undershoot. Further

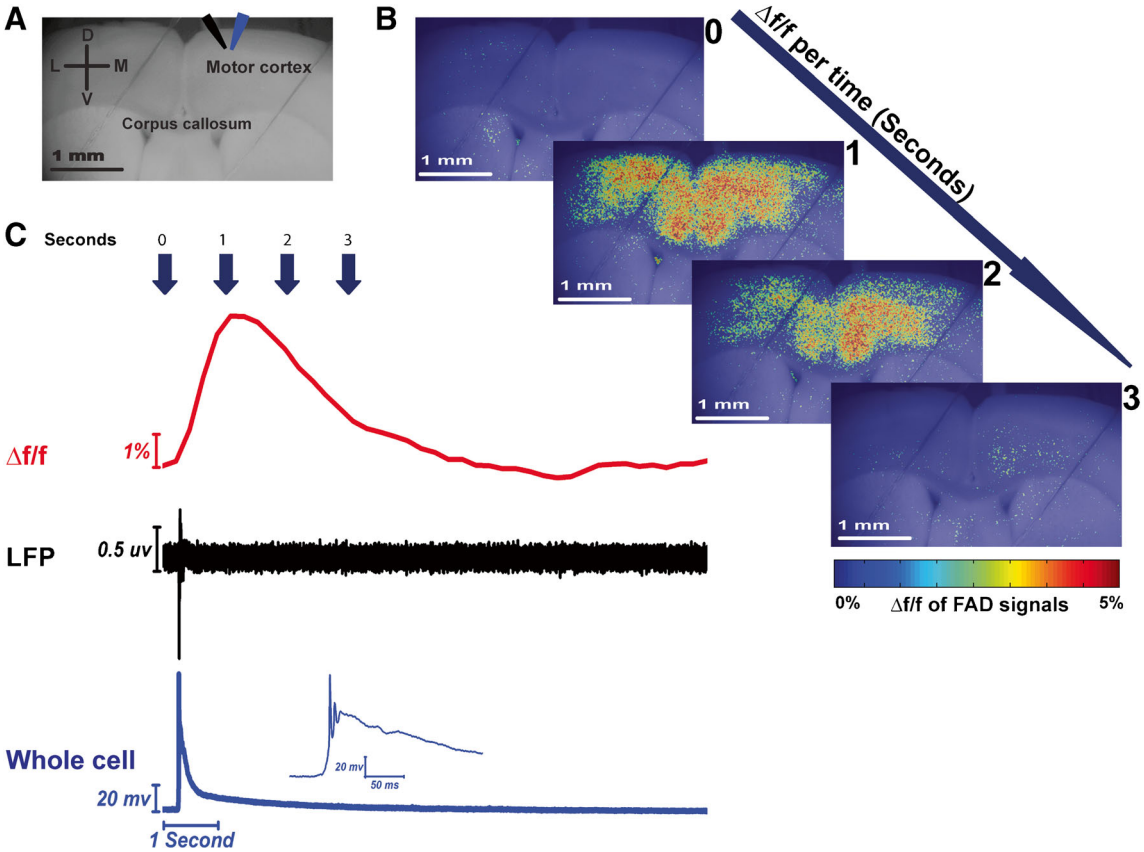

Fig. 3 Simultaneous flavoprotein imaging and electrophysiological recording of the SPD events evoked by SR-95531: **a** grayscale image of coronal brain slice showing the site of LFP (*black arrow*) and whole-cell recording (*blue arrow*); **b** pseudocolor heat maps of coronal brain slice showing the change of $\Delta f/f$ of FAD signals associated with SPD events per time; **c** time traces of $\Delta f/f$ of FAD (*top panel*), LFP (*middle panel*), and whole-cell recording (*bottom panel*) signals of SPD events occurring in the presence of 4 μM SR-95531

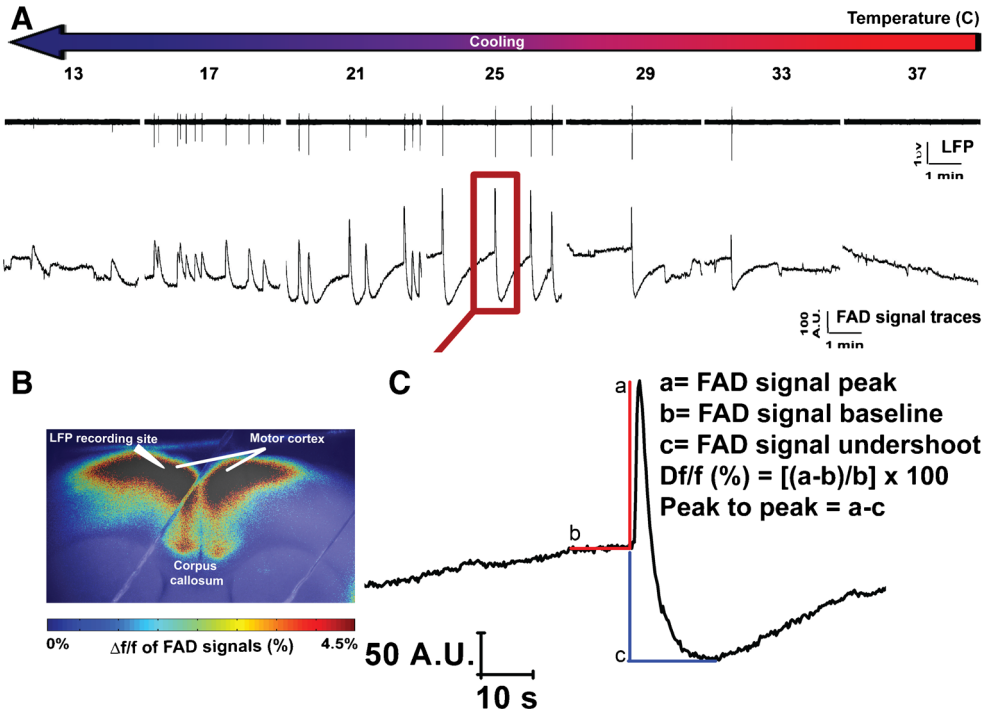

Fig. 4 Simultaneous measurement of LFP and FAD signals of SPD events occurring in the presence SR-95531 at different temperatures: **a** time traces of LFP (*top panel*) and those of FAD (*bottom panel*) signals associated with the SPD events in cortical layer 2/3 occurring in the presence of 4 μM of SR-95531 at different temperatures; **b** pseudocolor heat map of the average intensity of the $\Delta f/f$ of FAD signals associated with SPD events; **c** expansion of one FAD signal from FAD trace at 25 °C on panel **a** (*red square*) giving an expanded view for the different quantified components of FAD signal used for the analysis

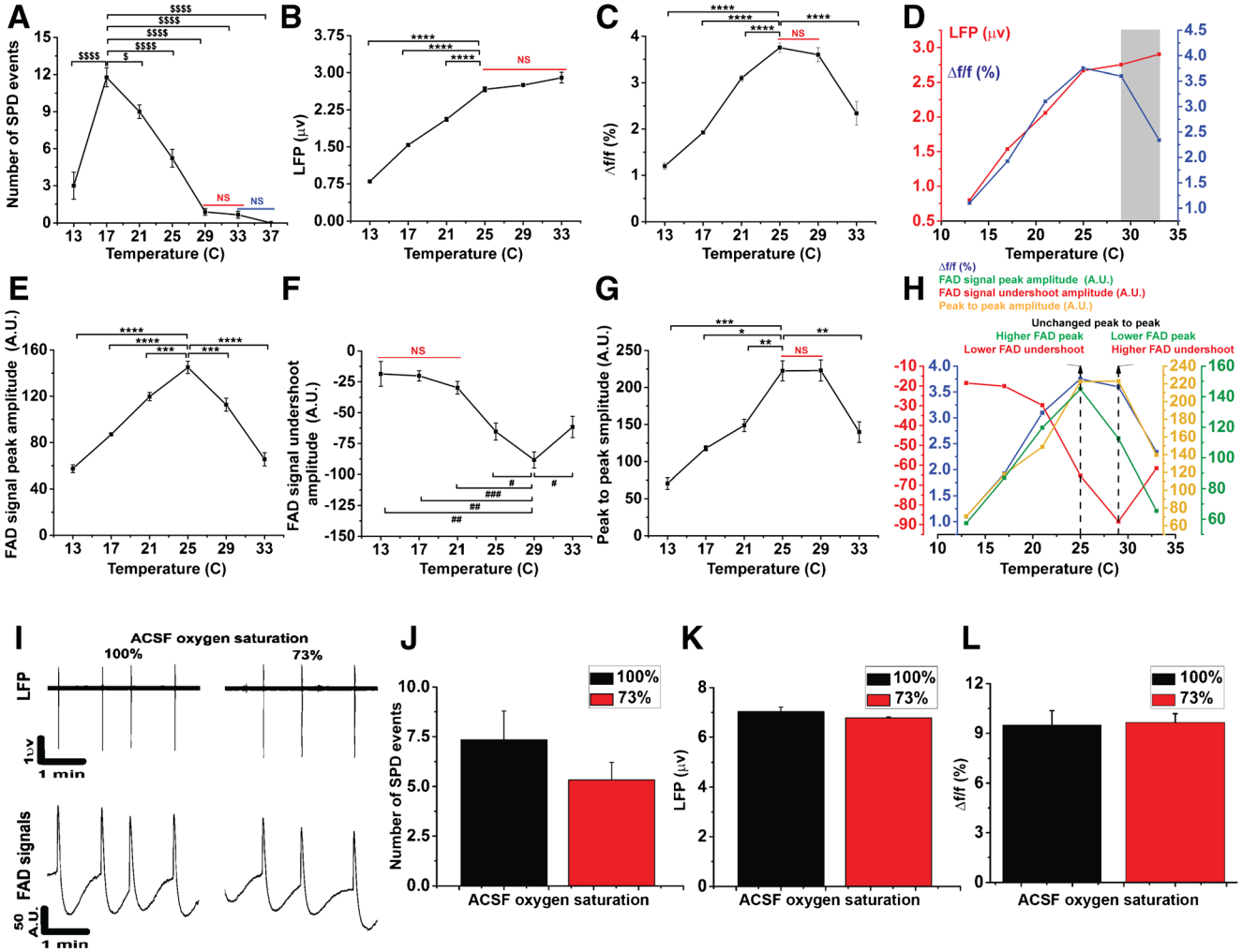

Fig. 5 Neurometabolic coupling is a temperature-dependent: **a**–**c**, **e**–**g** line plots showing temperature (*x*-axis) and the number of SPD events, LFP amplitudes, Δ*f*/*f* of FAD signals associated with SPD events, FAD signal peaks, FAD signal undershoots, peak to peak of FAD signals, respectively (*y*-axis); **d** merged plots of LFP and Δ*f*/*f* of FAD signals with temperature, *gray box* indicates decoupling zone; **h** merged plots of FAD signal components with temperature, *dotted black line* shows the maximum values of both FAD signal components; **i** time traces of LFP (*top panel*) and FAD (*bottom panel*) signals associated with SPD events recorded under 100 vs 73% oxygen saturated ACSF; **j**–**l** bar plots of the number of SPD events, LFP amplitude, and Δ*f*/*f* of FAD signals associated with SPD events, respectively, under 100% (*black bar*) vs 73% (*red bar*) oxygen saturated ACSF (for LFP and Δ*f*/*f*, $N = 9$, $n = 352$ and 322, respectively; for FAD signal peak, undershoot, and peak to peak, $N = 6$, $n = 199$, 67, 67, respectively; for LFP and Δ*f*/*f* in oxygen control experiment, $N = 3$, $n = 36$ and 34, respectively, in all cases one slice was used per mouse); post hoc, *vs 25 °C ($0.05 > p > 1 \times 10^{-4}$), **vs 25 °C ($1 \times 10^{-4} > p > 1 \times 10^{-7}$), ***vs 25 °C ($1 \times 10^{-7} > p > 1 \times 10^{-9}$), ****vs 25 °C ($p < 1 \times 10^{-9}$), #vs 29 °C ($0.05 > p > 1 \times 10^{-4}$), ##vs 29 °C ($1 \times 10^{-4} > p > 1 \times 10^{-7}$), ###vs 29 °C ($1 \times 10^{-7} > p > 1 \times 10^{-9}$); $vs 17 °C ($0.05 > p > 1 \times 10^{-4}$), $$vs 17 °C ($p < 1 \times 10^{-9}$); *NS*, non-significant difference between temperatures covered with a *solid line*

cooling decreased both FAD signal components significantly (Fig. 5e, f, $N = 6$, $n = 199$ and 67; $F(5, 198) = 60.5$ and $F(5, 66) = 11.8$; $p < 1 \times 10^{-9}$ and $=4.9 \times 10^{-8}$ for FAD signal peak and undershoot, respectively). The finding that FAD signal components have maximum excursions from baseline at different temperatures, and previous work suggesting that the FAD signal undershoot is caused by glial metabolism [82] could suggest temperature-dependent differences in neuronal compared to glial metabolism [13, 22, 80]. This hypothesis was further examined by combining the measurements of both FAD signal components (i.e., by measuring the peak to peak amplitude). Peak to peak values showed that the maximum absolute magnitude of FAD signal undershoot appeared to compensate for the drop of FAD signal peak at 29 °C. In contrast, the maximum of FAD signal peak compensated for the drop of the FAD signal undershoot at 25 °C before they decreased significantly by cooling further below 25 °C (Fig. 5g, $N = 6$, $n = 67$; $F(5, 66) = 11.9$, $P = 4.6 \times 10^{-8}$). Merging the plots of FAD signal components showed a strong correlation between Δ*f*/*f* and peak to peak of FAD signals (Fig. 5h). This figure also demonstrates how peak-to-peak measurements exhibited the compensation done by the FAD signal

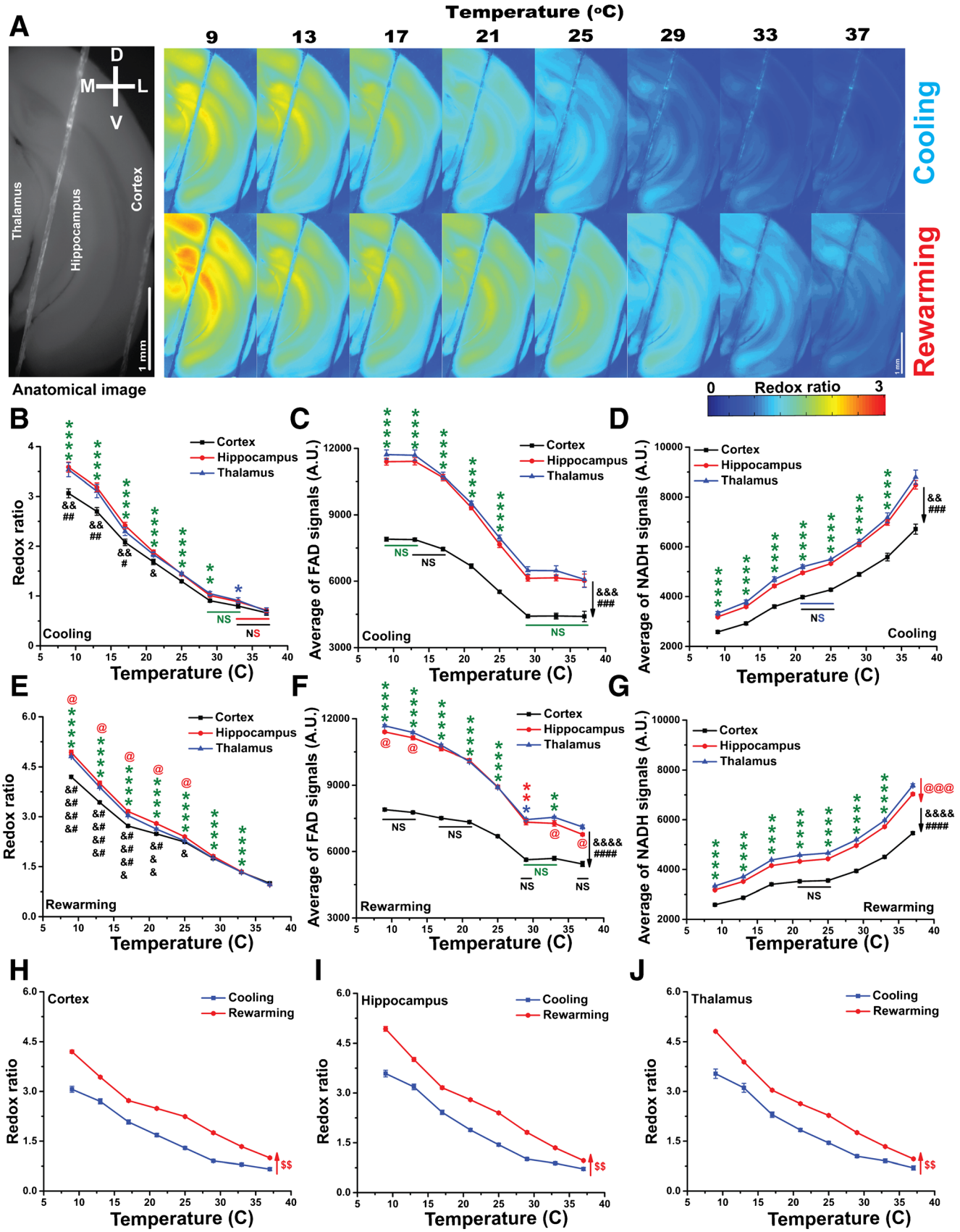
A
Temperature (°C)
9
13
17
21
25
29
33
37
D
M
L
V
Thalamus
Hippocampus
Cortex
1 mm
Cooling
Rewarming
Anatomical image
0
Redox ratio
3
B
C
D
Redox ratio
Average of FAD signals (A.U.)
Average of NADH signals (A.U.)
Cortex
Hippocampus
Thalamus
Cooling
Temperature (C)
E
F
G
Rewarming
H
I
J
Cooling
Rewarming
$$

◀ **Fig. 6** The metabolic redox ratio of the brain slice is temperature dependent: **a** pseudocolor heat maps of a coronal brain slice showing the negative relationship between temperature and the redox ratio under cooling (*top panel*) or rewarming (*bottom panel*); **b**–**d** line plots between temperature (*x*-axis) and redox ratio, FAD, and NADH signals, respectively (*y*-axis), of different brain structures under cooling; **e**–**g** line plots between temperature (*x*-axis) and redox ratio, FAD, and NADH signals, respectively (*y*-axis), of different brain structures under rewarming; **h**–**j** merged plots of the redox ratios of cortex, hippocampus, and thalamus, respectively, under cooling vs rewarming with temperature; $N = 4$, post hoc, *vs 37 °C ($0.05 > p > 1 \times 10^{-4}$), **vs 37 °C ($1 \times 10^{-4} > p > 1 \times 10^{-7}$), ****vs 37 °C ($p < 1 \times 10^{-9}$), $^{\#}$thalamus vs cortex ($0.05 > p > 1 \times 10^{-4}$), $^{\#\#}$thalamus vs cortex ($1 \times 10^{-4} > p > 1 \times 10^{-7}$), $^{\#\#\#}$thalamus vs cortex ($1 \times 10^{-7} > p > 1 \times 10^{-9}$), $^{\#\#\#\#}$thalamus vs cortex ($p < 1 \times 10^{-9}$), $^{\&}$hippocampus vs cortex ($0.05 > p > 1 \times 10^{-4}$), $^{\&\&}$hippocampus vs cortex ($1 \times 10^{-4} > p > 1 \times 10^{-7}$), $^{\&\&\&}$hippocampus vs cortex ($1 \times 10^{-7} > p > 1 \times 10^{-9}$), $^{\&\&\&\&}$hippocampus vs cortex ($p < 1 \times 10^{-9}$), $^{@}$hippocampus vs thalamus ($0.05 > p > 1 \times 10^{-4}$), $^{@@@}$hippocampus vs thalamus ($1 \times 10^{-7} > p > 1 \times 10^{-9}$), $^{\$\$}$vs cooling ($1 \times 10^{-4} > p > 1 \times 10^{-7}$), $^{\$\$\$}$vs cooling ($1 \times 10^{-7} > p > 1 \times 10^{-9}$); *NS*, non-significant difference between temperatures covered with a *solid line*. Statistical characters were *colored black* for cortex, *red* for hippocampus or rewarming, and *green* for all brain structures

undershoot for the diminished FAD signal peak and vice versa at 25–29 °C (dotted black lines).

To determine whether the lowered oxygen solubility at 37 °C was responsible for the temperature-dependent changes described above, LFP and FAD signals were also measured during SPD events using ACSF solutions of different oxygen saturations (100 vs 73%) at room temperature (Fig. 5i). The number of SPD events (Fig. 5j, $N = 3$, t (4) = 1.17, $p = 0.3$), LFP amplitude (Fig. 5k, $N = 3$, $n = 36$, t (34) = −1.57, $p = 0.12$), and $\Delta f/f$ (Fig. 5l, $N = 3$, $n = 34$, t (32) = 0.67, $p = 0.50$) of FAD signals associated with SPD events showed no significant difference between 100 and 73% oxygen saturated ACSF solutions. Therefore, as before, the impact of the change of oxygen tension mediated by temperature was minimal.

Temperature-dependent profile of redox ratios

Redox ratio is an established marker for the metabolic state of different tissue types including the brain [24, 65, 89, 96]. To determine if the temperature-dependent changes in FAD signals and neurometabolic signals described above were related to changes in resting redox state, both raw FAD and NADH endogenous fluorescence signals of brain slices were measured at different temperatures. A control experiment examining the effect of temperature on the fluorescence of FAD and NADH compounds showed that the fluorescence signals of both compounds had a negative relationship with temperature (data not shown) as previously reported for FAD [53]. As such, the endogenous FAD and NADH fluorescence signals of brain slices were normalized accordingly. The redox ratios (FAD/NADH) of the imaged regions of the cerebral cortex, hippocampus, and thalamus were then calculated. Under cooling, the redox ratio of all brain structures showed a temperature-dependent negative relationship with temperature (Fig. 6a, b), though the FAD and NADH signals showed opposite profiles. Upon cooling, whereas, FAD signals showed a negative relationship with temperature, NADH signals showed a positive relationship with lowest baseline values in the cerebral cortex for both signals (Fig. 6c, d). Similar general patterns were seen with rewarming for redox ratio, FAD, and NADH signals (Fig. 6a, e–g). Interestingly, thalamus and hippocampus had a higher redox ratio than cortex at 9–21 °C regardless the direction of temperature change (Fig. 6b, e). In all three brain structures, redox ratios remained higher at all temperatures with rewarming retaining the same negative relationship with temperature (Fig. 6h–j). Table 1 shows the results of the statistical analysis of this section.

Cooling normalizes the oxidative state of brain tissue under hypoxia

As shown above (Fig. 6a–g), high temperatures shifted the metabolism of the brain slice towards its reduced state indicated by lowering redox ratio, lowering FAD, and raising NADH signals, which mimics hypoxic like conditions [68]. In contrast, cooling was able to simulate a more oxidized state of the brain slice. To address the impact of cooling to normalize the state of brain tissue under hypoxia, the redox ratio of coronal brain slices was measured under different oxygen tensions. The induction of hypoxic conditions is expected to diminish oxidative phosphorylation and shift the metabolic reactions towards glycolysis [63, 69]. This shift is expected to lead to a reduction in FAD fluorescence signals, an increase in NADH fluorescence signals, and lowering the redox ratio. As expected, it was observed that the redox ratio of cortex, hippocampus, and thalamus under hypoxia was significantly lower than normal conditions at all temperatures with retention of the negative relationship with temperature (Fig. 7a–d, $N = 3$; F (1, 12) = 1368, 3308, and 1598; $p = 7.2 \times 10^{-4}$, 3.0×10^{-4}, and 6.2×10^{-4}, condition effect, F (6, 12) = 4.6, 20.0, and 9.29; $p = 0.01$, 1.3×10^{-5}, and 6.2×10^{-4}, interaction between temperature and condition for cortex, hippocampus, and thalamus, respectively). The interpolation between the redox ratio curves under hypoxia and normal conditions (the horizontal solid blue line) showed a tissue-specific temperature to which that tissue must be cooled to normalize the redox ratio. Cooling to 22.3 and 23 °C was required to return the cortex and thalamus to their baseline values, respectively. However, the hippocampus required further cooling to 20.8 °C to attain the same level of normalization of redox state (Fig. 7b–d). The interaction between the redox ratio of the brain structures and temperature showed a significant difference under normoxic conditions at 13–25 °C (Fig. 7e, $N = 3$, f (12, 24) = 14.0, $p = 4.7 \times 10^{-8}$). In contrast, the redox ratio of all brain structures showed no significant difference under hypoxia (Fig. 7f, $N = 3$, f (12, 24) = 0.92, $p = 0.54$). Based on these data, and given that hypoxia results in

Table 1 The statistical analysis within temperature, brain structures, and the interaction for redox ratios, FAD signals, and NADH signals under cooling versus rewarming

	Condition	Effect within	*N*	*f*	*p*
Redox ratio	Cooling (Fig. 6b)	Temperature	4	$f(7, 42) = 261.3$	$p < 1 \times 10^{-9}$
		Brain structure		$f(2, 42) = 205.6$	$p = 2.9 \times 10^{-6}$
		Temperature × brain structure		$f(14, 42) = 7.5$	$p = 1.5 \times 10^{-7}$
	Rewarming (Fig. 6e)	Temperature		$f(7, 42) = 2039.6$	$p < 1 \times 10^{-9}$
		Brain structure		$f(2, 42) = 345.0$	$p = 6.4 \times 10^{-7}$
		Temperature × brain structure		$f(14, 42) = 26.9$	$p < 1 \times 10^{-9}$
	Cooling × rewarming	Cortex (Fig. 6h)		$f(1, 21) = 764.6$	$p = 1.0 \times 10^{-4}$
		Hippocampus (Fig. 6i)		$f(1, 21) = 1369.0$	$p = 4.3 \times 10^{-5}$
		Thalamus (Fig. 6j)		$f(1, 21) = 985.9$	$p = 7.0 \times 10^{-5}$
FAD signals	Cooling (Fig. 6c)	Temperature		$f(7, 42) = 177.1$	$p < 1 \times 10^{-9}$
		Brain structure		$f(2, 42) = 47{,}714.7$	$p < 1 \times 10^{-9}$
		Temperature × brain structure		$f(14, 42) = 19.4$	$p < 1 \times 10^{-9}$
	Rewarming (Fig. 6f)	Temperature		$f(7, 42) = 688.6$	$p < 1 \times 10^{-9}$
		Brain structure		$f(2, 42) = 95{,}153.0$	$p < 1 \times 10^{-9}$
		Temperature × brain structure		$f(14, 42) = 53.1$	$p < 1 \times 10^{-9}$
NADH signals	Cooling (Fig. 6d)	Temperature		$f(7, 42) = 220.3$	$p < 1 \times 10^{-9}$
		Brain structure		$f(2, 42) = 4817.4$	$p < 1 \times 10^{-9}$
		Temperature × brain structure		$f(14, 42) = 23.6$	$p < 1 \times 10^{-9}$
	Rewarming (Fig. 6g)	Temperature		$f(7, 42) = 2422.1$	$p < 1 \times 10^{-9}$
		Brain structure		$f(2, 42) = 24{,}882.6$	$p < 1 \times 10^{-9}$
		Temperature × brain structure		$f(14, 42) = 75.2$	$p < 1 \times 10^{-9}$

an increase in NADH and a reduction in FAD fluorescence signals, we considered that the calculated redox ratio under hypoxic conditions to be the lowest attainable redox ratio under our experimental conditions. The percent of oxidative capacity of all the brain structures showed a temperature-dependent inverted-U shape with a maximum level around room temperature (Fig. 7h, $N = 3$, $F(2, 24) = 978$, $P = 4.1 \times 10^{-6}$, within brain structures, $F(6, 24) = 4.0$, $P = 0.018$, within temperature, $F(12, 24) = 2.9$, $P = 0.011$, for interaction). This finding is consistent with our previous finding of $\Delta f/f$ of FAD signals associated with synaptic activity (Fig. 2b, e) and supports our assumption that oxidative capacity is maximal at intermediate temperatures. Although there was no significant difference in percent of oxidative capacity between the three brain structures across all temperatures, the interaction between brain structures and temperatures showed that the percent of oxidative capacity of hippocampus is greater than cortex only at 17–25°.

Discussion

Summary

A substantial change of FAD peak or NADH dip ($\Delta f/f$) associated with neuronal activity was observed to show strong temperature dependence. During electrical stimulation and during spontaneous events, maximal FAD and NADH signal deviations from baseline were seen at temperatures between 21 and 29 °C. With increasing temperature (≥29 °C), the diminishment in magnitude of the FAD peak or NADH dip (the oxidation phase) was associated with the emergence of FAD undershoot and NADH overshoot (the reduction phase) to form a biphasic profile of FAD and NADH signals. In contrast, at cold temperatures (≤25 °C) electrically evoked signals showed a monophasic profile of FAD and NADH signals. Further cooling below 21 °C reduced the magnitude of this monophasic profile without any other changes. Synaptic activity in the cortex measured with LFPs was generally matched with FAD signals, except at temperatures above 29 °C, where FAD signals dropped off while synaptic responses were retained. The inverted-U shape of the FAD signal deviations may be explained by temperature dependence of resting FAD levels, whose levels decreased with increasing temperature. Finally, hypoxia caused strong changes in FAD and NADH levels that were normalized by cooling to room temperature where most of brain slice studies were conducted. However, the degree of cooling required was greater than that used clinically, and the hippocampus required the greatest degree of cooling, suggesting that hippocampal tissue may be more sensitive to hypoxia than thalamus or cortex. These data suggest that the coupling between synaptic activity and metabolic activity in the brain is temperature-dependent, and have implications for the use of FAD and NADH fluorescence signals as an imaging tool.

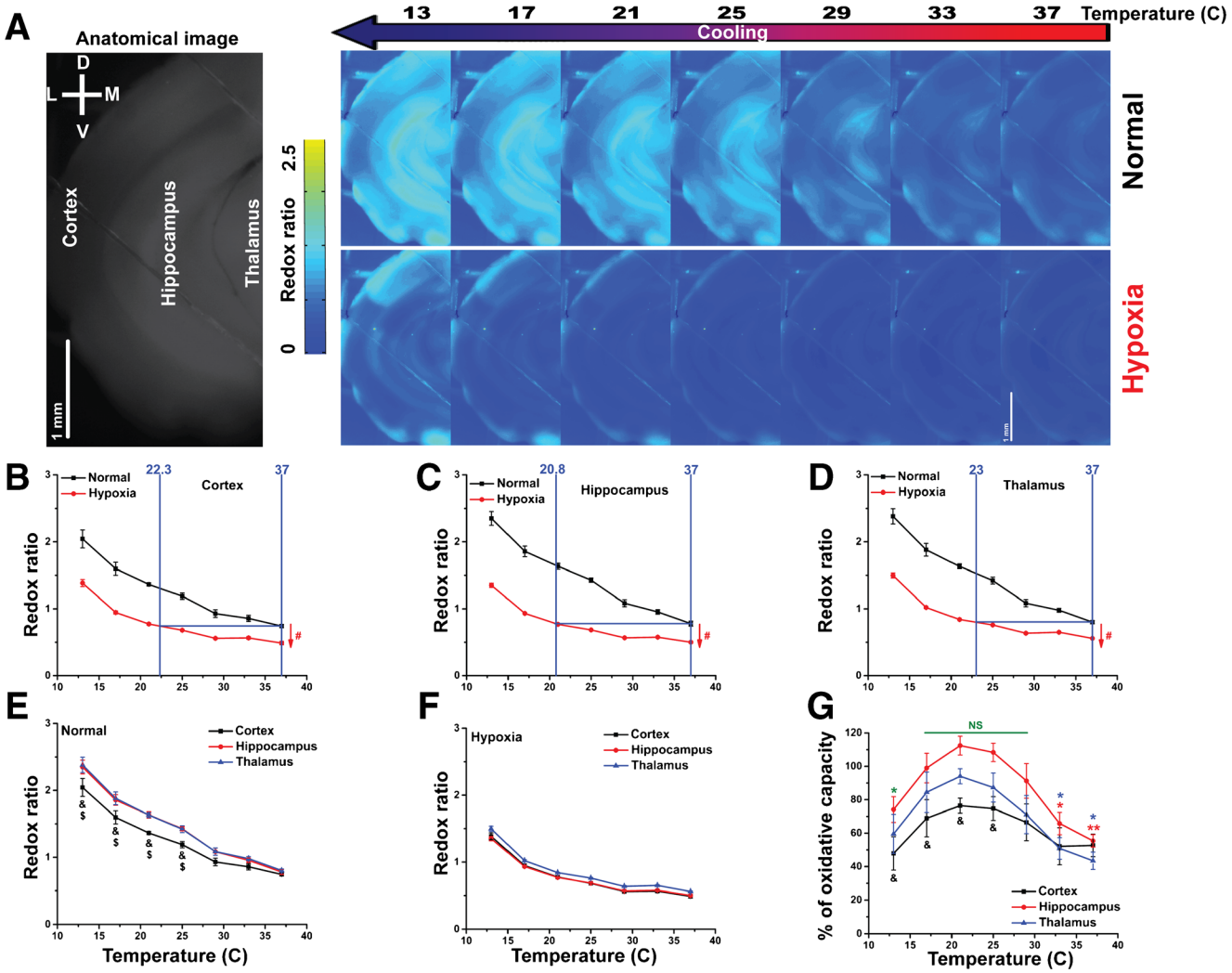

Fig. 7 Hypothermia normalizes the oxidative states of the brain slice under hypoxia: **a** pseudocolor heat maps of a coronal brain slice showing the change of the redox ratio of the tissue under hypoxia (*bottom panel*) vs normal condition (*top of panel*); **b**–**d** merged plots of the redox ratios of cortex, hippocampus, and thalamus, respectively, under normal vs hypoxia with temperature; The quantification of redox ratios of the three brain structures under hypoxia. **e** Line plots between temperature (*x*-axis) and redox ratio (*y*-axis) of different brain structures under normal condition; **f** line plots between temperature (*x*-axis) and redox ratio (*y*-axis) of different brain structures under hypoxia; **g** line plots between temperature (*x*-axis) and % of oxidative capacity of different brain structures; $N = 3$; post hoc, *vs 25 °C ($0.05 > p > 1 \times 10^{-4}$), **vs 25 °C ($1 \times 10^{-4} > p > 1 \times 10^{-7}$), $^{\#}$vs normal ($0.05 > p > 1 \times 10^{-4}$), $^{\$}$thalamus vs cortex ($0.05 > p > 1 \times 10^{-4}$), $^{\&}$hippocampus vs cortex ($0.05 > p > 1 \times 10^{-4}$); *NS*, non-significant difference between temperatures covered with a *solid line*. Statistical characters were *colored black* for cortex, *red* for hippocampus or hypoxia, *blue* for thalamus, and *green* for all brain structures

Methodological considerations

The biological factors that are sensitive to temperature in the whole animal, such as systemic or cerebral blood flow, blood pressure, and the affinity of oxygen to hemoglobin [3, 52, 72, 108], were not present in the current preparation. As such, in the current study, it is not possible to account for the complex physiological environment of the brain and the network between brain and periphery. This limitation is mitigated by the fact that by removing these variables, the brain slice was nourished by a continuous supply of nutrients, electrolytes, and oxygen which permits a greater degree of control of physiological parameters than does a whole-animal preparation. In this study, 600 μm auditory thalamocortical brain slice was used to retain the connectivity between auditory thalamus and cortex, though slices at this thickness may create metabolic gradients across tissue depth [7, 20, 40]. We note that we have previously established that slices cut and perfused in the manners described in the Methods section, which include bi-level perfusion at high flow rates, maintain high tissue viability throughout the inner portions of the slice [104]. In addition, given the relatively poor penetration of blue and ultraviolet light into scattering tissues, we assume

that the majority of the optical signals were generated from the surface 200 μm of the slice [2, 109], where there is a good oxygen diffusion regardless the animal age [21, 40].

An additional consideration is the rate of temperature change and physiological assessments used. The current study was focused on steady-state temperature change, giving the specimen time to accommodate after the temperature change. It is possible that during the equilibration time, cellular compensatory mechanisms could be triggered, which would be reflected in physiological and imaging measurements made in this study. Other investigators have used a more dynamic approach, measuring physiological changes that occur transiently after temperature change [15]. Interestingly, the results of the dynamic approach were generally similar to the results shown here. In the dynamic model used by others previously [15], the sudden temperature drop from 35 to 29 °C increased hippocampal neuronal excitability. Similarly, our model showed no SPD events at 37 °C, but these events started to appear at 33 °C, and the frequency of events increased by further cooling. The negative relationship between temperature and oxygen solubility has long been reported in both biological and artificial solutions [7, 10, 33]. Since our experiments were conducted in ACSF, the temperature-induced change of oxygen tension in ACSF could possibly be a confounding factor. Our data diminished this possibility by showing that exposure to a lower oxygen concentration that is normally induced by 37 °C at room temperature did not have a significant impact on FAD signals evoked by electrical stimulation (Fig. 2j, k) or spontaneously by SR-95531 (Fig. 5i–l) compared to control.

As a non-invasive method, optical imaging of endogenous fluorescence signals like FAD/NADH has a major advantage to study living tissue without interfering its biochemical and physiological state. However, there are some pitfalls associated with this technique that should be taken into consideration. Photo damage and photo-bleaching associated with NADH imaging, where UV light is required for NADH excitation, could have a negative impact on the integrity of the tissue and the quality of the signal to noise ratio [36, 54]. For this reason, NADH imaging was conducted for short periods of time (2 min for electrical evoked activity and 10 s for redox ratio per each temperature point). In addition, only FAD imaging (which uses a longer excitation wavelength than NAD imaging) was used to track SPD events, when a longer time (3–5 min per each temperature point) was needed. Finally, the spatial resolution of FAD and NADH imaging, as used in the current study, does not permit determination of the cellular sources of the measured signals. It may be useful ultimately to understand the cell types (neurons vs glia, subtypes of each) responsible for the imaging signals. Two-photon microscopy may ultimately permit this to happen, but to our knowledge, has not be used to measure FAD or NADH signals from brain slices previously.

Implications

Despite these methodological concerns, our data showed a strong agreement with previous studies. Temperature-mediated change in LFP amplitude was seen previously [1]. Here, the investigators observed that LFP amplitudes remained at their highest level at 31 °C before they decayed with cooling of hippocampal slices isolated from guinea pig [1]. Similarly, it was reported that temperature range (21–23 °C) held the highest peak of EPSPs evoked by a stimulating current to layer 2/3 of cat visual cortex [103]. The high frequency of SPD events induced by cooling was consistent with the work done on cultured hippocampal cells or hippocampal slices of the Swiss OF1 mouse, where cooling near to 28 °C induced the increase of the cellular excitability of hippocampal neurons [15]. Our data showed that low temperatures kept the electron carriers at their oxidized state (↑ FAD and ↓ NADH), while high temperature kept them at their reduced state (↑ NADH and ↓ FAD) (Fig. 6c, f, d, g). Similarly, the induction of more reduction reactions by high temperatures could explain the appearance of the reduction phase of both FAD and NADH following the oxidation phase to form the electrically evoked biphasic transient change of FAD and NADH signals. Such biphasic profile of FAD and NADH signals was shown before by other studies conducted above 33 °C [35, 46, 93]. In contrast, cooling, which induced more oxidation, drove only a monophasic transient change, which represents the oxidation reactions only, of FAD and NADH signals (Fig. 1e).

Both temperatures (13 and 37 °C) showed low versus no neuronal activity, respectively, which could implicate the lack of the energy needed to meet neuronal demands. However, the temperature change away from 13 and 37 °C mobilized FAD and NADH which could explain the inverted-U shape of the $\Delta f/f$ of FAD signals (Figs. 2b, e and 4c) and NADH signals (Fig. 2c, f) of maximum values at 25 °C. A similar temperature was reported to hold the maximum ATP production of the isolated rat liver mitochondria [17]. Therefore, plotting Δf only (FAD signal peak, Fig. 5e) versus temperature superimposed the same inverted-U-shaped profile as $\Delta f/f$ (Fig. 5h). The thermoregulation of oxidative phosphorylation could support our findings. It was reported that increasing temperature increased both respiration and phosphorylation rates in isolated muscle mitochondria of houseflies and rats [41, 85]. However, increasing the temperature above 31 °C in houseflies or 35 °C in rats uncoupled the two processes and reduced mitochondrial oxidative phosphorylation efficiency [41, 85]. Similarly, isolated rat brain mitochondria showed that the respiratory control ratio, which is obtained by dividing state 3 (phosphorylating respiration) by state 4 (non-phosphorylating respiration), had a temperature-dependent inverted-U shape profile within range with a highest value at (20–25 °C) [31].

Our data showed that LFP amplitude of SPD evoked by SR-95531 remained at its maximum level at high temperature which was decoupled to the $\Delta f/f$ of FAD signals associated with this neuronal activity (derived by the oxidative phosphorylation) (Fig. 5d). Interestingly, the rat brain slices were reported to have a higher anaerobic glycolysis with increasing the temperature with a maximum value at 38 °C [6] which could indicate the increase in NADH fluorescence signals at high temperatures. Such higher anaerobic glycolysis could be a compensatory mechanism to meet the essential energy demand of brain slices. Energy insult situations were reported to drive the brain to undergo anaerobic respiration [88]. Further, under normal conditions, visual stimulation has been shown to increase the blood flow and glucose to the visual cortex without an increase in oxygen consumption, suggesting that brain activity can be partially met by anaerobic glycolysis [4]. Interestingly, the peak frequency of gamma oscillation of rat hippocampal slices was increased by increasing the temperature above 28 °C. The same effect was attained by adding lactate after induction of glucose deprivation conditions to the hippocampal slice [86]. Lactate is known to be produced under brain anaerobic respiration [16]. The current study showed that different brain structures could have different metabolic responses elicited by cooling. Both thalamus and hippocampus were more responsive to the temperature change below 25 °C in normoxic conditions compared to cortex in two separate experiments (Figs. 6b, e and 7e). However, hippocampus had a highest oxidative capacity which could be because of its higher metabolic demands, as previously observed [35, 47]. Such effects made the hippocampus more vulnerable to the hypoxic insults, a result which is supported by previous studies [11, 74]. The current study showed the positive impact of hypothermia to normalize the redox ratio under hypoxia, which implicated the protective role of hypothermia against oxidative insults. This finding was consistent with numerous experimental studies showing the positive impact of hypothermia on metabolism and survival rates [19, 28, 45, 75, 106]. Clinically, hypothermia is well recognized for its therapeutic impact in the treatment of some brain injuries [104] such as anoxic brain injury due to cardiac arrest [5, 37, 73], and hypoxic-ischemic neonatal encephalopathy [25, 90].

Our data could also have significant methodological implications for imaging studies. The correlation between the higher blood flow carrying oxygen, uptake, and utilization of glucose and lactate upon neuronal activity is called neurometabolic coupling which has been reported by numerous in vitro [48, 61, 76, 102] and in vivo [9, 77, 94] studies. In addition, most functional imaging techniques including PET, fMRI, and others were developed based on neurometabolic coupling to measure brain activity in normal versus pathological conditions [26, 64, 83]. In contrast, our data showed a neurometabolic decoupling above 29 °C in brain slice. While FAD signals were used to track the neuronal activity in vivo, where the core body temperature of the subject was kept at 37–37.5 °C [32, 34], our study showed an inability to detect FAD signals at 37 °C. Given that the neurometabolic coupling at 25 °C was associated with the maximum oxidative capacity and the maximum metabolic change evoked by the neuronal activity, 37 °C, the optimal temperature in vivo, could possibly be shifted to lower temperature in vitro. This finding could have a great impact on the reliability of all in vitro experiments done at 37 °C to mimic the physiological conditions. Although FAD imaging used to track the metabolic status or the neuronal activity of brain slices has been conducted at different temperatures across different studies, no studies were conducted above 36 °C, which could support our assumption [27, 44, 59, 70, 96]. Despite the positive impact of cooling on metabolism, our results showed a low metabolic capacity at very low temperatures. This finding implicates a safe zone of cooling (21–29 °C) which could mimic the clinical therapeutic cooling zone.

Conclusion

The current data demonstrate the effect of temperature on the metabolism and the neurometabolic coupling of mouse brain slice. Neuronal and metabolic activities were found to be decoupled with temperature-dependent profile which could be caused by the effect of temperature on the basal metabolism of brain tissue. The higher metabolic performance of brain tissue that was held at 25 °C which could have a positive experimental impact in the determination of the suitable temperature to conduct brain slice experiments. In addition, the protective role of cooling against hypoxia was shown, which supports the potential of therapeutic hypothermia for the protection against brain oxidative insults.

Acknowledgements The Carle Neuroscience Institute supported the work. D.A.L. was supported by DC013073. The authors thank Dr. Eugene Kiyatkin (NIH), Dr. Robert Gennis (University of Illinois), Dr. Sanjiv Sinha (University of Illinois), Dr. Naoum Issa (University of Chicago), Dr. Jan Ramirez (Seattle Children's Hospital), and Dr. Alfredo Garcia (Seattle Children's Hospital) for their suggestions.

Compliance with ethical standards

Conflict of interest The authors declare that they have no conflicts of interest.

References

1. Aihara H, Okada Y, Tamaki N (2001) The effects of cooling and rewarming on the neuronal activity of pyramidal neurons in guinea pig hippocampal slices. Brain Res 893:36–45
2. Al-Juboori SI, Dondzillo A, Stubblefield EA, Felsen G, Lei TC, Klug A (2013) Light scattering properties vary across different

regions of the adult mouse brain. PLoS One 8:e67626. doi:10.1371/journal.pone.0067626
3. Alva N, Palomeque J, Carbonell T (2013) Oxidative stress and antioxidant activity in hypothermia and rewarming: can RONS modulate the beneficial effects of therapeutic hypothermia? Oxidative Med Cell Longev 2013:957054. doi:10.1155/2013/957054
4. Belanger M, Allaman I, Magistretti PJ (2011) Brain energy metabolism: focus on astrocyte-neuron metabolic cooperation. Cell Metab 14:724–738. doi:10.1016/j.cmet.2011.08.016
5. Bernard SA, Gray TW, Buist MD, Jones BM, Silvester W, Gutteridge G, Smith K (2002) Treatment of comatose survivors of out-of-hospital cardiac arrest with induced hypothermia. N Engl J Med 346:557–563. doi:10.1056/NEJMoa003289
6. Burlington RF, Wiebers JE (1967) The effect of temperature on glycolysis in brain and skeletal muscle from a hibernator and a non-hibernator. Physiol Zool 40:201–206
7. Bingmann D, Kolde G (1982) PO2-profiles in hippocampal slices of the guinea pig. Exp Brain Res 48:89–96
8. Buzatu S (2009) The temperature-induced changes in membrane potential. Riv Biol 102:199–217
9. Chih CP, Lipton P, Roberts EL Jr (2001) Do active cerebral neurons really use lactate rather than glucose? Trends Neurosci 24:573–578
10. Christoforides C, Hedley-Whyte J (1969) Effect of temperature and hemoglobin concentration on solubility of O_2 in blood. J Appl Physiol 27:592–596
11. Cooper JM, Gadian DG, Jentschke S, Goldman A, Munoz M, Pitts G, Banks T, Chong WK, Hoskote A, Deanfield J, Baldeweg T, de Haan M, Mishkin M, Vargha-Khadem F (2015) Neonatal hypoxia, hippocampal atrophy, and memory impairment: evidence of a causal sequence. Cereb Cortex 25:1469–1476. doi:10.1093/cercor/bht332
12. Costa C, Belcastro V, Tozzi A, Di Filippo M, Tantucci M, Siliquini S, Autuori A, Picconi B, Spillantini MG, Fedele E, Pittaluga A, Raiteri M, Calabresi P (2008) Electrophysiology and pharmacology of striatal neuronal dysfunction induced by mitochondrial complex I inhibition. J Neurosci 28:8040–8052. doi:10.1523/JNEUROSCI.1947-08.2008
13. Coutinho V, Mutoh H, Knopfel T (2004) Functional topology of the mossy fibre-granule cell—Purkinje cell system revealed by imaging of intrinsic fluorescence in mouse cerebellum. Eur J Neurosci 20:740–748. doi:10.1111/j.1460-9568.2004.03533.x
14. Cruikshank SJ, Rose HJ, Metherate R (2002) Auditory thalamocortical synaptic transmission in vitro. J Neurophysiol 87:361–384
15. de la Pena E, Malkia A, Vara H, Caires R, Ballesta JJ, Belmonte C, Viana F (2012) The influence of cold temperature on cellular excitability of hippocampal networks. PLoS One 7:e52475. doi:10.1371/journal.pone.0052475
16. Dong B (1997) Progresses in the study of ultrasonics in China, 1997. Zhonghua Yi Xue Za Zhi 77:927–929
17. Dufour S, Rousse N, Canioni P, Diolez P (1996) Top-down control analysis of temperature effect on oxidative phosphorylation. Biochem J 314(Pt 3):743–751
18. Edelstein A, Amodaj N, Hoover K, Vale R, Stuurman N (2010) Computer control of microscopes using microManager. Curr Protoc Mol Biol Chapter 14:Unit14 20. doi:10.1002/0471142727.mb1420s92
19. Erecinska M, Thoresen M, Silver IA (2003) Effects of hypothermia on energy metabolism in mammalian central nervous system. J Cereb Blood Flow Metab 23:513–530. doi:10.1097/01.WCB.0000066287.21705.21
20. Foster KA, Beaver CJ, Turner DA (2005) Interaction between tissue oxygen tension and NADH imaging during synaptic stimulation and hypoxia in rat hippocampal slices. Neuroscience 132:645–657. doi:10.1016/j.neuroscience.2005.01.040
21. Galeffi F, Somjen GG, Foster KA, Turner DA (2011) Simultaneous monitoring of tissue PO_2 and NADH fluorescence during synaptic stimulation and spreading depression reveals a transient dissociation between oxygen utilization and mitochondrial redox state in rat hippocampal slices. J Cereb Blood Flow Metab 31:626–639. doi:10.1038/jcbfm.2010.136
22. Gao W, Chen G, Reinert KC, Ebner TJ (2006) Cerebellar cortical molecular layer inhibition is organized in parasagittal zones. J Neurosci 26:8377–8387. doi:10.1523/JNEUROSCI.2434-06.2006
23. Garofalo O, Cox DW, Bachelard HS (1988) Brain levels of NADH and NAD+ under hypoxic and hypoglycaemic conditions in vitro. J Neurochem 51:172–176
24. Gerich FJ, Funke F, Hildebrandt B, Fasshauer M, Muller M (2009) H(2)O(2)-mediated modulation of cytosolic signaling and organelle function in rat hippocampus. Pflugers Arch 458:937–952. doi:10.1007/s00424-009-0672-0
25. Gluckman PD, Wyatt JS, Azzopardi D, Ballard R, Edwards AD, Ferriero DM, Polin RA, Robertson CM, Thoresen M, Whitelaw A, Gunn AJ (2005) Selective head cooling with mild systemic hypothermia after neonatal encephalopathy: multicentre randomised trial. Lancet 365:663–670. doi:10.1016/S0140-6736(05)17946-X
26. Gosseries O, Demertzi A, Noirhomme Q, Tshibanda J, Boly M, Op de Beeck M, Hustinx R, Maquet P, Salmon E, Moonen G, Luxen A, Laureys S, De Tiege X (2008) Functional neuroimaging (fMRI, PET and MEG): what do we measure? Rev Med Liege 63:231–237
27. Grosser E, Hirt U, Janc OA, Menzfeld C, Fischer M, Kempkes B, Vogelgesang S, Manzke TU, Opitz L, Salinas-Riester G, Muller M (2012) Oxidative burden and mitochondrial dysfunction in a mouse model of Rett syndrome. Neurobiol Dis 48:102–114. doi:10.1016/j.nbd.2012.06.007
28. Hagerdal M, Harp J, Siesjo BK (1975) Effect of hypothermia upon organic phosphates, glycolytic metabolites, citric acid cycle intermediates and associated amino acids in rat cerebral cortex. J Neurochem 24:743–748
29. Hajos N, Mody I (2009) Establishing a physiological environment for visualized in vitro brain slice recordings by increasing oxygen supply and modifying aCSF content. J Neurosci Methods 183:107–113. doi:10.1016/j.jneumeth.2009.06.005
30. Hajos N, Ellender TJ, Zemankovics R, Mann EO, Exley R, Cragg SJ, Freund TF, Paulsen O (2009) Maintaining network activity in submerged hippocampal slices: importance of oxygen supply. Eur J Neurosci 29:319–327. doi:10.1111/j.1460-9568.2008.06577.x
31. Hillered L, Chan PH (1988) Effects of arachidonic acid on respiratory activities in isolated brain mitochondria. J Neurosci Res 19:94–100. doi:10.1002/jnr.490190113
32. Hishida R, Kudoh M, Shibuki K (2014) Multimodal cortical sensory pathways revealed by sequential transcranial electrical stimulation in mice. Neurosci Res 87:49–55. doi:10.1016/j.neures.2014.07.004
33. Hodgman C (1958-1959) Handbook of chemistry and physics—fortieth edition. Chemical Rubber Publishing, Co., Cleveland
34. Horie M, Tsukano H, Takebayashi H, Shibuki K (2015) Specific distribution of non-phosphorylated neurofilaments characterizing each subfield in the mouse auditory cortex. Neurosci Lett 606:182–187. doi:10.1016/j.neulet.2015.08.055
35. Huchzermeyer C, Albus K, Gabriel HJ, Otahal J, Taubenberger N, Heinemann U, Kovacs R, Kann O (2008) Gamma oscillations and spontaneous network activity in the hippocampus are highly sensitive to decreases in pO_2 and concomitant changes in

mitochondrial redox state. J Neurosci 28:1153–1162. doi:10.1523/JNEUROSCI.4105-07.2008
36. Husson TR, Issa NP (2009) Functional imaging with mitochondrial flavoprotein autofluorescence theory, practice, and applications. Front Neurosci 221–253. doi:10.1201/9781420076851
37. Hypothermia after Cardiac Arrest Study G (2002) Mild therapeutic hypothermia to improve the neurologic outcome after cardiac arrest. N Engl J Med 346:549–556. doi:10.1056/NEJMoa012689
38. Ivanov A, Zilberter Y (2011) Critical state of energy metabolism in brain slices: the principal role of oxygen delivery and energy substrates in shaping neuronal activity. Front Neuroenerg 3:9. doi:10.3389/fnene.2011.00009
39. Ivanov AI, Malkov AE, Waseem T, Mukhtarov M, Buldakova S, Gubkina O, Zilberter M, Zilberter Y (2014) Glycolysis and oxidative phosphorylation in neurons and astrocytes during network activity in hippocampal slices. J Cereb Blood Flow Metab 34:397–407. doi:10.1038/jcbfm.2013.222
40. Ivanov AI, Bernard C, Turner DA (2015) Metabolic responses differentiate between interictal, ictal and persistent epileptiform activity in intact, immature hippocampus in vitro. Neurobiol Dis 75:1–14. doi:10.1016/j.nbd.2014.12.013
41. Jarmuszkiewicz W, Woyda-Ploszczyca A, Koziel A, Majerczak J, Zoladz JA (2015) Temperature controls oxidative phosphorylation and reactive oxygen species production through uncoupling in rat skeletal muscle mitochondria. Free Radic Biol Med 83:12–20. doi:10.1016/j.freeradbiomed.2015.02.012
42. Ji S, Chance B, Stuart BH, Nathan R (1977) Two-dimensional analysis of the redox state of the rat cerebral cortex in vivo by NADH fluorescence photography. Brain Res 119:357–373
43. Johnston D, Brown TH (1981) Giant synaptic potential hypothesis for epileptiform activity. Science 211:294–297
44. Jotty K, Shuttleworth CW, Valenzuela CF (2015) Characterization of activity-dependent changes in flavoprotein fluorescence in cerebellar slices from juvenile rats. Neurosci Lett 584:17–22. doi:10.1016/j.neulet.2014.09.052
45. Kaibara T, Sutherland GR, Colbourne F, Tyson RL (1999) Hypothermia: depression of tricarboxylic acid cycle flux and evidence for pentose phosphate shunt upregulation. J Neurosurg 90:339–347. doi:10.3171/jns.1999.90.2.0339
46. Kann O, Kovacs R, Njunting M, Behrens CJ, Otahal J, Lehmann TN, Gabriel S, Heinemann U (2005) Metabolic dysfunction during neuronal activation in the ex vivo hippocampus from chronic epileptic rats and humans. Brain 128:2396–2407. doi:10.1093/brain/awh568
47. Kann O, Huchzermeyer C, Kovacs R, Wirtz S, Schuelke M (2011) Gamma oscillations in the hippocampus require high complex I gene expression and strong functional performance of mitochondria. Brain 134:345–358. doi:10.1093/brain/awq333
48. Kasischke KA, Vishwasrao HD, Fisher PJ, Zipfel WR, Webb WW (2004) Neural activity triggers neuronal oxidative metabolism followed by astrocytic glycolysis. Science 305:99–103. doi:10.1126/science.1096485
49. Kim JA, Connors BW (2012) High temperatures alter physiological properties of pyramidal cells and inhibitory interneurons in hippocampus. Front Cell Neurosci 6:27. doi:10.3389/fncel.2012.00027
50. Kim DY, Vallejo J, Rho JM (2010) Ketones prevent synaptic dysfunction induced by mitochondrial respiratory complex inhibitors. J Neurochem 114:130–141. doi:10.1111/j.1471-4159.2010.06728.x
51. Kimura R, Ma LY, Wu C, Turner D, Shen JX, Ellsworth K, Wakui M, Maalouf M, Wu J (2012) Acute exposure to the mitochondrial complex I toxin rotenone impairs synaptic long-term potentiation in rat hippocampal slices. CNS Neurosci Ther 18:641–646. doi:10.1111/j.1755-5949.2012.00337.x
52. Koehn J, Kollmar R, Cimpianu CL, Kallmunzer B, Moeller S, Schwab S, Hilz MJ (2012) Head and neck cooling decreases tympanic and skin temperature, but significantly increases blood pressure. Stroke 43:2142–2148. doi:10.1161/STROKEAHA.112.652248
53. Kowalska A, Gyugos M, Szego D, Pineda AL, Ayala D, Xu Y, Hughes N, Tito A, Jabłonska J (2007) The thermal scanning fluorescence study on the conformational stability of glucose oxidase (GOD) from Aspergillus niger. Food Chem Biotechnol 71:35–48
54. Kubota Y, Kamatani D, Tsukano H, Ohshima S, Takahashi K, Hishida R, Kudoh M, Takahashi S, Shibuki K (2008) Transcranial photo-inactivation of neural activities in the mouse auditory cortex. Neurosci Res 60:422–430. doi:10.1016/j.neures.2007.12.013
55. Lee JC, Callaway JC, Foehring RC (2005) Effects of temperature on calcium transients and Ca^{2+}-dependent afterhyperpolarizations in neocortical pyramidal neurons. J Neurophysiol 93:2012–2020. doi:10.1152/jn.01017.2004
56. Li LZ, Xu HN, Ranji M, Nioka S, Chance B (2009) Mitochondrial redox imaging for cancer diagnostic and therapeutic studies. J Innov Opt Health Sci 2:325–341. doi:10.1142/S1793545809000735
57. Llano DA, Theyel BB, Mallik AK, Sherman SM, Issa NP (2009) Rapid and sensitive mapping of long-range connections in vitro using flavoprotein autofluorescence imaging combined with laser photostimulation. J Neurophysiol 101:3325–3340. doi:10.1152/jn.91291.2008
58. Llano DA, Turner J, Caspary DM (2012) Diminished cortical inhibition in an aging mouse model of chronic tinnitus. J Neurosci 32:16141–16148. doi:10.1523/JNEUROSCI.2499-12.2012
59. Llano DA, Slater BJ, Lesicko AM, Stebbings KA (2014) An auditory colliculothalamocortical brain slice preparation in mouse. J Neurophysiol 111:197–207. doi:10.1152/jn.00605.2013
60. Ma H, Cai Q, Lu W, Sheng ZH, Mochida S (2009) KIF5B motor adaptor syntabulin maintains synaptic transmission in sympathetic neurons. J Neurosci 29:13019–13029. doi:10.1523/JNEUROSCI.2517-09.2009
61. Magistretti PJ (2006) Neuron-glia metabolic coupling and plasticity. J Exp Biol 209:2304–2311. doi:10.1242/jeb.02208
62. Magistretti PJ, Allaman I (2015) A cellular perspective on brain energy metabolism and functional imaging. Neuron 86:883–901. doi:10.1016/j.neuron.2015.03.035
63. Malthankar-Phatak GH, Patel AB, Xia Y, Hong S, Chowdhury GM, Behar KL, Orina IA, Lai JC (2008) Effects of continuous hypoxia on energy metabolism in cultured cerebro-cortical neurons. Brain Res 1229:147–154. doi:10.1016/j.brainres.2008.06.074
64. Mandeville ET, Ayata C, Zheng Y, Mandeville JB (2017) Translational MR neuroimaging of stroke and recovery. Transl Stroke Res 8:22–32. doi:10.1007/s12975-016-0497-z
65. Mayevsky A (1984) Brain NADH redox state monitored in vivo by fiber optic surface fluorometry. Brain Res 319:49–68
66. Mayevsky A, Chance B (1974) Repetitive patterns of metabolic changes during cortical spreading depression of the awake rat. Brain Res 65:529–533
67. Mayevsky A, Chance B (1982) Intracellular oxidation-reduction state measured in situ by a multichannel fiber-optic surface fluorometer. Science 217:537–540
68. Mayevsky A, Zarchin N, Friedli CM (1982) Factors affecting the oxygen balance in the awake cerebral cortex exposed to spreading depression. Brain Res 236:93–105
69. Michiels C (2004) Physiological and pathological responses to hypoxia. Am J Pathol 164:1875–1882. doi:10.1016/S0002-9440(10)63747-9

70. Middleton JW, Kiritani T, Pedersen C, Turner JG, Shepherd GM, Tzounopoulos T (2011) Mice with behavioral evidence of tinnitus exhibit dorsal cochlear nucleus hyperactivity because of decreased GABAergic inhibition. Proc Natl Acad Sci U S A 108:7601–7606. doi:10.1073/pnas.1100223108
71. Mori K, Maeda M, Miyazaki M, Iwase H (1998) Effects of mild (33 degrees C) and moderate (29 degrees C) hypothermia on cerebral blood flow and metabolism, lactate, and extracellular glutamate in experimental head injury. Neurol Res 20:719–726
72. Mrozek S, Vardon F, Geeraerts T (2012) Brain temperature: physiology and pathophysiology after brain injury. Anesthesiol Res Pract 2012:989487. doi:10.1155/2012/989487
73. Nielsen N, Wetterslev J, Cronberg T, Erlinge D, Gasche Y, Hassager C, Horn J, Hovdenes J, Kjaergaard J, Kuiper M, Pellis T, Stammet P, Wanscher M, Wise MP, Aneman A, Al-Subaie N, Boesgaard S, Bro-Jeppesen J, Brunetti I, Bugge JF, Hingston CD, Juffermans NP, Koopmans M, Kober L, Langorgen J, Lilja G, Moller JE, Rundgren M, Rylander C, Smid O, Werer C, Winkel P, Friberg H, Investigators TTMT (2013) Targeted temperature management at 33 degrees C versus 36 degrees C after cardiac arrest. N Engl J Med 369:2197–2206. doi:10.1056/NEJMoa1310519
74. Osborne NN, Tobin AB, Ghazi H (1988) Role of inositol trisphosphate as a second messenger in signal transduction processes: an essay. Neurochem Res 13:177–191
75. Palladino WG, Proctor HJ, Jobsis FF (1983) Effect of hypothermia during hypoxic hypotension on cerebral metabolism. J Surg Res 34:388–393
76. Pellerin L, Magistretti PJ (1994) Glutamate uptake into astrocytes stimulates aerobic glycolysis: a mechanism coupling neuronal activity to glucose utilization. Proc Natl Acad Sci U S A 91:10625–10629
77. Phillips AA, Chan FH, Zheng MM, Krassioukov AV, Ainslie PN (2016) Neurovascular coupling in humans: physiology, methodological advances and clinical implications. J Cereb Blood Flow Metab 36:647–664. doi:10.1177/0271678X15617954
78. Quinn PJ (1988) Effects of temperature on cell membranes. Symp Soc Exp Biol 42:237–258
79. Ranji M, Kanemoto S, Matsubara M, Grosso MA, Gorman JH 3rd, Gorman RC, Jaggard DL, Chance B (2006) Fluorescence spectroscopy and imaging of myocardial apoptosis. J Biomed Opt 11:064036. doi:10.1117/1.2400701
80. Reinert KC, Dunbar RL, Gao W, Chen G, Ebner TJ (2004) Flavoprotein autofluorescence imaging of neuronal activation in the cerebellar cortex in vivo. J Neurophysiol 92:199–211. doi:10.1152/jn.01275.2003
81. Reinert KC, Gao W, Chen G, Ebner TJ (2007) Flavoprotein autofluorescence imaging in the cerebellar cortex in vivo. J Neurosci Res 85:3221–3232. doi:10.1002/jnr.21348
82. Reinert KC, Gao W, Chen G, Wang X, Peng YP, Ebner TJ (2011) Cellular and metabolic origins of flavoprotein autofluorescence in the cerebellar cortex in vivo. Cerebellum 10:585–599. doi:10.1007/s12311-011-0278-x
83. Ricker JH, Hillary FG, DeLuca J (2001) Functionally activated brain imaging (O-15 PET and fMRI) in the study of learning and memory after traumatic brain injury. J Head Trauma Rehabil 16:191–205
84. Roy CS, Sherrington CS (1890) On the regulation of the blood-supply of the brain. J Physiol 11(85–158):117
85. Sacktor B, Sanborn R (1956) The effect of temperature on oxidative phosphorylation with insect flight muscle mitochondria. J Biophys Biochem Cytol 2:105–107
86. Schneider J, Lewen A, Ta TT, Galow LV, Isola R, Papageorgiou IE, Kann O (2015) A reliable model for gamma oscillations in hippocampal tissue. J Neurosci Res 93:1067–1078. doi:10.1002/jnr.23590
87. Schuh RA, Matthews CC, Fishman PS (2008) Interaction of mitochondrial respiratory inhibitors and excitotoxins potentiates cell death in hippocampal slice cultures. J Neurosci Res 86:3306–3313. doi:10.1002/jnr.21772
88. Schurr A, Rigor BM (1998) Brain anaerobic lactate production: a suicide note or a survival kit? Dev Neurosci 20:348–357
89. Sepehr R, Staniszewski K, Maleki S, Jacobs ER, Audi S, Ranji M (2012) Optical imaging of tissue mitochondrial redox state in intact rat lungs in two models of pulmonary oxidative stress. J Biomed Opt 17:046010. doi:10.1117/1.JBO.17.4.046010
90. Shankaran S, Laptook AR, Ehrenkranz RA, Tyson JE, SA MD, Donovan EF, Fanaroff AA, Poole WK, Wright LL, Higgins RD, Finer NN, Carlo WA, Duara S, Oh W, Cotten CM, Stevenson DK, Stoll BJ, Lemons JA, Guillet R, Jobe AH, National Institute of Child H, Human Development Neonatal Research N (2005) Whole-body hypothermia for neonates with hypoxic-ischemic encephalopathy. N Engl J Med 353:1574–1584. doi:10.1056/NEJMcps050929
91. Shibuki K, Hishida R, Murakami H, Kudoh M, Kawaguchi T, Watanabe M, Watanabe S, Kouuchi T, Tanaka R (2003) Dynamic imaging of somatosensory cortical activity in the rat visualized by flavoprotein autofluorescence. J Physiol 549:919–927. doi:10.1113/jphysiol.2003.040709
92. Shuttleworth CW (2010) Use of NAD(P)H and flavoprotein autofluorescence transients to probe neuron and astrocyte responses to synaptic activation. Neurochem Int 56:379–386. doi:10.1016/j.neuint.2009.12.015
93. Shuttleworth CW, Brennan AM, Connor JA (2003) NAD(P)H fluorescence imaging of postsynaptic neuronal activation in murine hippocampal slices. J Neurosci 23:3196–3208
94. Sibson NR, Dhankhar A, Mason GF, Rothman DL, Behar KL, Shulman RG (1998) Stoichiometric coupling of brain glucose metabolism and glutamatergic neuronal activity. Proc Natl Acad Sci U S A 95:316–321
95. Slater BJ, Fan AY, Stebbings KA, Saif MT, Llano DA (2015) Modification of a colliculo-thalamocortical mouse brain slice, incorporating 3-D printing of chamber components and multi-scale optical imaging. J Vis Exp doi:10.3791/53067
96. Stebbings KA, Choi HW, Ravindra A, Caspary DM, Turner JG, Llano DA (2016) Ageing-related changes in GABAergic inhibition in mouse auditory cortex, measured using in vitro flavoprotein autofluorescence imaging. J Physiol 594:207–221. doi:10.1113/JP271221
97. Steriade M, Amzica F (1999) Intracellular study of excitability in the seizure-prone neocortex in vivo. J Neurophysiol 82:3108–3122
98. Vanzetta I, Flynn C, Ivanov AI, Bernard C, Benar CG (2010) Investigation of linear coupling between single-event blood flow responses and interictal discharges in a model of experimental epilepsy. J Neurophysiol 103:3139–3152. doi:10.1152/jn.01048.2009
99. Varela C, Llano DA, Theyel BB (2012) An introduction to in vitro slice approaches for the study of neuronal circuitry. NeuroMethods 67:103–125. doi:10.1007/7657_2011_19
100. Vazquez AL, Masamoto K, Fukuda M, Kim SG (2010) Cerebral oxygen delivery and consumption during evoked neural activity. Front Neuroenerg 2:11. doi:10.3389/fnene.2010.00011
101. Vazquez AL, Fukuda M, Kim SG (2012) Evolution of the dynamic changes in functional cerebral oxidative metabolism from tissue mitochondria to blood oxygen. J Cereb Blood Flow Metab 32:745–758. doi:10.1038/jcbfm.2011.198
102. Viswanathan A, Freeman RD (2007) Neurometabolic coupling in cerebral cortex reflects synaptic more than spiking activity. Nat Neurosci 10:1308–1312. doi:10.1038/nn1977

103. Volgushev M, Vidyasagar TR, Chistiakova M, Yousef T, Eysel UT (2000) Membrane properties and spike generation in rat visual cortical cells during reversible cooling. J Physiol 522(Pt 1):59–76
104. Wang H, Wang B, Normoyle KP, Jackson K, Spitler K, Sharrock MF, Miller CM, Best C, Llano D, Du R (2014) Brain temperature and its fundamental properties: a review for clinical neuroscientists. Front Neurosci 8:307. doi:10.3389/fnins.2014.00307
105. Xu G, Perez-Pinzon MA, Sick TJ (2003) Mitochondrial complex I inhibition produces selective damage to hippocampal subfield CA1 in organotypic slice cultures. Neurotox Res 5:529–538
106. Yager JY, Asselin J (1996) Effect of mild hypothermia on cerebral energy metabolism during the evolution of hypoxic-ischemic brain damage in the immature rat. Stroke 27:919–925 discussion 926
107. Yaron-Jakoubovitch A, Koch C, Segev I, Yarom Y (2013) The unimodal distribution of sub-threshold, ongoing activity in cortical networks. Front Neural Circuits 7:116. doi:10.3389/fncir.2013.00116
108. Yenari M, Kitagawa K, Lyden P, Perez-Pinzon M (2008) Metabolic downregulation: a key to successful neuroprotection? Stroke 39:2910–2917. doi:10.1161/STROKEAHA.108.514471
109. Yona G, Meitav N, Kahn I, Shoham S (2016) Realistic numerical and analytical modeling of light scattering in brain tissue for optogenetic applications(1,2,3). eNeuro 3. doi:10.1523/ENEURO.0059-15.2015